POLITECNICO DI TORINO

Corso di Laurea Magistrale

In Ingegneria Biomedica

Tesi di Laurea Magistrale

Automatic segmentation algorithm and Texture Analysis for tumor tissues on Mammary Magnetic Resonance Imaging (MMRI)

Tutor:
Prof. Filippo Molinari

Examinee:
Stefania Zara

July 2018

SOMMARIO

L'attività di ricerca di questo progetto di tesi ha portato allo sviluppo di un sistema di Computer Aided Diagnosis (CAD) per la segmentazione e l'analisi delle lesioni tumorali del seno su immagini di Risonanza Magnetica Mammaria. Una volta terminato il contornamento, dalle regioni segmentate vengono estrapolati parametri geometrici e di Texture Analysis che facilitano la diagnosi da parte del medico.

Il processo consiste di 5 step fondamentali realizzati mediante algoritmo Matlab:

1. *Pre-processing dell'immagine*, per ciascun paziente sono state fornite le immagini dinamiche con contrasto (DCE-MRI) in sei scansioni temporali, una pre-contrasto e 5 post-contrasto (195 immagini per scansione). Delle sei scansioni temporali si selezionano quelle di maggior interesse clinico e da queste si ricavano le sottratte. Per gli esami pre-terapia neoadiuvante viene applicata una variazione del contrasto con lo scopo di evidenziare le regioni maggiormente perfuse. Nel caso delle scansioni post-trattamento, essendo i tessuti tumorali meno perfusi, non viene variato il contrasto onde evitare una sottostima della regione tumorale.

2. *Contornamento dell'area da esaminare*, per minimizzare la regione di ricerca delle lesioni tumorali, dall'immagine originale si ricavano due sotto-immagini contenenti i due seni. Su ciascuna di esse viene poi applicato un algoritmo di segmentazione del contorno (Level-set) seguito da un algoritmo di Thinning. Queste operazioni vengono effettuate per la rimozione degli elementi che non sono di interesse clinico in questa applicazione quali organi interni e la pelle del seno.

3. *Segmentazione delle lesioni tumorali*, sulla regione da investigare viene applicato un algoritmo di segmentazione a doppia soglia (Seeded Region Growing) per l'identificazione e il contornamento delle regioni sospette. Utilizzando l'algoritmo di Mean Maximum Raw Thresholding (MMRT) viene costruita una maschera binaria contenente solo le aree aventi intensità maggiore del valore di MMRT. Dalla maschera si ricava l'immagine originale in toni di grigio e per ogni regione si calcola il valore di densità corrispondente; l'area con densità maggiore è quella che viene riconosciuta come regione sospetta (SR). La prima soglia viene selezionata come valore massimo di intensità della regione scelta, e utilizzata per determinare il Seed iniziale dell'algoritmo. Il valore della seconda soglia invece viene scelto come la differenza tra l'intensità media della regione sospetta e quella del suo vicinato. Questa operazione viene ripetuta separatamente per i due seni.

4. *Analisi euristica*, per una riduzione dei falsi positivi le zone segmentate vengono valutate ed eventualmente scartate sulla base di criteri geometrici e di intensità dei pixel. Essendo la morfologia delle lesioni tumorali molto variabile, la valutazione geometrica si ripropone di discriminare solo le segmentazioni con una forma prevalentemente allungata generalmente corrispondente ai vasi. Per una maggiore selettività sono stati implementati due criteri geometrici:

- Valutazione delle segmentazioni piane: se la forma risulta essere prevalentemente allungata allora viene scartata.
- Valutazione delle segmentazioni volumetriche: la regione segmentata viene confrontata con il volume di una geometria regolare, se il rapporto tra le due supera una certa soglia fissata allora la lesione viene rimossa.

Il criterio geometrico non è però sufficiente a discriminare forme più diversificate, per questo motivo è stato aggiunto un criterio di discriminazione che si basa sulla valutazione della perfusione dei tessuti. Per ciascun volume segmentato viene ricavata la curva rappresentativa dell'assorbimento del contrasto nelle diverse scansioni temporali. Le lesioni tumorali hanno un assorbimento più rapido rispetto agli altri tessuti, sfruttando questa caratteristica si riescono dunque a discriminare i falsi positivi con maggiore selettività.

5. *Caratterizzazione parametrica*, per ciascuna regione segmentata si calcolano informazioni geometriche e parametri clinici (Texture Analysis) utili ai fini diagnostici. Queste caratteristiche vengono calcolate sia sulle segmentazioni piane che su quelle volumetriche. Regioni aventi geometrie sospette devono essere analizzate indipendentemente dai valori degli altri parametri, più la forma è complessa maggiore sarà la probabilità che la lesione sia maligna. Per quanto concerne i parametri di Texture Analysis è stato osservato, da diversi studi, come questi possano essere di aiuto ai fini diagnostici per facilitare i clinici nella discriminazione tra lesione benigne e maligne.

L'algoritmo è stato costruito su 10 pazienti e successivamente validato su altri 5, di questi ultimi sono stati forniti diversi esami post-trattamento per valutare l'efficacia della terapia nel tempo. Per la validazione sono state valutate sia la capacità dell'algoritmo di identificare le regioni sospette all'interno della mammella, sia la qualità della segmentazione delle ROI. Le immagini sono state fornite dall'ospedale Borgo Trento di Verona in collaborazione con Tecnologie Avanzate S.r.l.

Contents

Chapter 1

Introduction

In 2003, 5.3 million of men and 4.7 million of women were estimated to develop a malignant tumor annually and 6.2 million would die from the disease. In 2014, 14.1 million people were expected to develop cancer annually. Breast cancer is the second leading cause of cancer death among women, this affect more than one in 10 women and accounts for 28.8% of female cancer. Several studies have shown that there is 1.4% of probability for a 40-year-old woman of being diagnosed with breast cancer over the next 10 years [1] [2] [3].

Mammography is usually a good method for breast lesions screening but in compromised mammogram patients MRI study is usually recommended, the most common cases are related to breast preservation therapies and difficult histology due to lobular carcinoma or ductal carcinoma in situ. MRI are also used in patients with dense breast, silicon augmented breast, breasts with scarring. Magnetic Resonance Imaging (MRI) has been chosen as imaging modalities because of its sensitivity and a threefold improvement in specificity over conventional imaging. The better performances of this technique are used to improve the quality of diagnosis and effectiveness of the treatment of breast cancer [3] [4] .

Computer Aided Diagnosis (CAD) systems has an increasingly important role in healthcare applications. The main purpose is to assist radiologists in evaluation of clinical images to provide a 'second opinion' and optimize clinical diagnosis time. CAD studies improve diagnosis accuracy of radiologist, reduce diseases missing due to fatigue and improve inter- and intra-reader variability, with a minimum error related to the device failure [5].

There are several methods for breast lesions segmentation in MRI, these can be categorized into two main groups: contour-based segmentation and classification-based segmentation.

Segmentation methods based on classifiers can be divided into three main categories: supervised, semi-supervised and unsupervised. Supervised methods, such as Neural Network and Support Vector Machine [6] [7] [8], are those with greater accuracy but require a large amount of data difficult, expensive and slow to find. Non-supervised methods on the other hand do not require training data but have much lower performance, e.g. Markov Random Field and Fuzzy C-means and others [9] [10] [11]. A good

compromise between these categories is semi-supervised approach that maintain high accuracy, but it still requires labelled data, a semi-supervised method application is the one proposed by Azmi R. et al. [12].

Contour-based segmentation, as it is not operator dependent, can reduce analysis time and provide more repeatable results. Only few studies have presented algorithms for automatic lesion detection in breast MRI. Vignati et al. (2011) developed a segmentation method based on multiscale 3D Sato's vessel enhancement filter for vessels intensity identification, this value is used to remove all vessel from segmented regions, then an empirically threshold is determined to segment only tumoral regions. The advantage of this algorithm is that it works both on fat-sat and non-fat sat DCE-MRI, but it use mean intensity projection image over time (mIPT) and this could underestimate lesion size, error that could lead to a wrong lesion classification [13]. Renz et al. (2012) implemented a fully automated CAD system based on a hierarchical 3D Gaussian pyramid, each voxel of a lower level was linked to a voxel of the next upper level depending on the intensity similarities, the limitation of this work is related to the difficult to identify nonmass-like lesion [14]. Gubern-Mérida et al. (2014) performed an algorithm that identifies the candidate lesions using blob and relative enhancement voxel features. In this work spatial information were provided by probabilistic atlases the results of this system are less accurate because of the use of only one seed for lesion detection [15].

To overcome some of the limitations just listed, in this study we investigate a fully automated segmentation algorithm for tumor breast, referring to the work of Al-Faris et al. [16]. The main objective of the system proposed by Al-Faris et al. is the identification of lesions on DCE image without user interaction; this study consist of single image segmentation and does not include an evaluation of the results to reduce the number of false positives. In our work we tried to solve these restrictions, the built system receives as input the folder with all DCE images which consist of six-time scans (195 images per scan), the algorithm processes all images and after it works on each slice individually. For the lesion identification and contouring a Seeded Region Growing is applied, the threshold selection is totally automatized based on gray level intensity of the image. After lesion segmentation we reconstruct the regions volume and several considerations are applied to distinguish lesion from non-lesion. At the end of the suspected regions selection, to facilitate the diagnosis by the radiologist, geometrical variables and texture analysis were determined for the selected regions characterization. Morphological parameters provide further information relevant for prognosis, suspicious morphology should be followed and controlled, regardless of other features [17] [18]. Texture analysis (TA) otherwise give information about gray level distribution on the selected region, these parameters are related to different histological types, tumor grades and micro-vessel distributions. These clinical features provide prognostic and predictive information, useful also for molecular subtypes classification [19].

Chapter 2

Breast Magnetic Resonance Imaging

Magnetic Resonance Imaging (MRI) plays an important role in clinical care, it is a scanning method that obtains tomographic images of the human body through a magnetic field. MRI is generally considered non-harmful to the patient, the information given by the magnetic resonance images are different from those of the other imaging methods, it is possible to discriminate between tissues, based on their biochemical composition. With MR there are images of the body sections on three different planes (axial, coronal, sagittal). The main disadvantages of this technique are costs and time necessary for images acquisition.

Breast MRI is a complementary radiological examination of conventional imaging (mammography and ultrasound), it can be used to have functional information of the breast tissue noninvasively. This technique has a relevant role in monitoring of neoadjuvant chemotherapy, several studies shown that parameters deriving from pharmacokinetic models can be used as imaging biomarkers, it is crucial in assessing the patient's response to therapy and to evaluate the size of the lesion in patients with low response [20] [21] [22].

Figure 1. MR system with MammoTrack trolley [23].

2.1 Breast image acquisition

To minimize inhomogeneity, in breast MRI, magnets have a high B, higher than 1T. The acquisitions are multi-phase and they have a high signal-to-noise ratio. Fat-suppression is used in routine magnetic resonance imaging for several reasons:

- Suppression of the signal from adipose tissue
- Reduction of chemical shift artifact
- Improvement of the contrast uptake visualization
- Characterization of tissues.

Signal in non-adipose tissues is not affected by fat-suppression but signal-to-noise ratio in adipose tissue decrease. The major disadvantage is that an inhomogeneity in the radio-frequency field can reduce the effectiveness of the fat-suppression which leads to water-suppression and therefore to a poor quality of the signal.

Coils used are bilateral multi-channel and volumetric, able to acquire 3D images in the three planes with high spatial resolution and with thin layers (maximum 3mm). Coils are positioned on the tabletop with the aperture to the magnet, correct positioning of the breast coil is crucial to limit the number of artifacts.
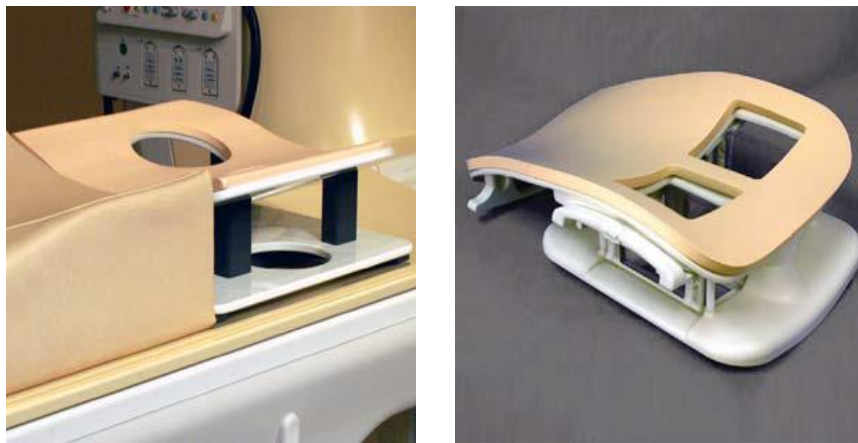

Figure 2. SENSE breast coil with 4 element phased-array coil and one coil receive only (left), SENSE breast coil with 7 element phased-array coil and one coil receive only (right) [23].

The basic images produced in breast MRI includes:

- T2 sequences
- T1 gradient-echo
- Injected dynamic 3D sequences

T2 sequences give useful information about signal analysis and anatomy of the breast, this scan performed without fat saturation guarantee a good predictive value for a benign cyst, while the sequences acquired with fat saturation are useful in detecting small tumors.
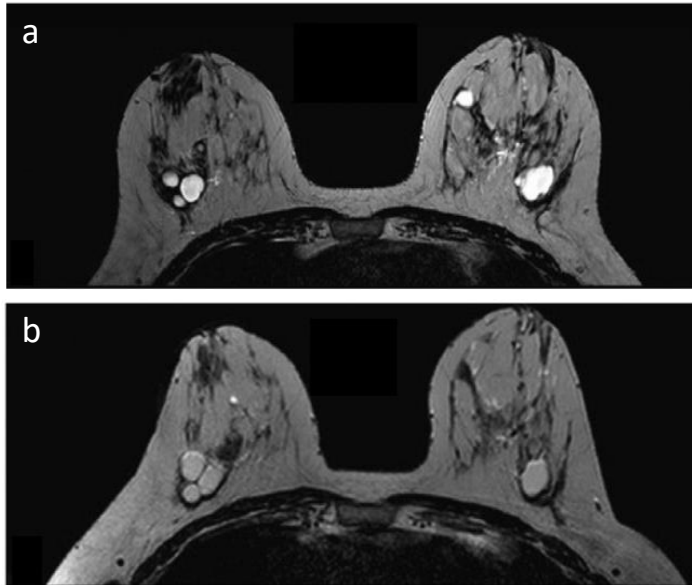
Figure 3. Comparison of a T2-wighted axial sequence on 1.5T (a) and 3.0T (b) machines [24].

The T1-weighted sequences are useful in detecting the fat component within the lesion, which is an index of the benign nature of the tumor. This type of scan allows also to detect metal markers inserted at the end of the biopsy, to be able to see this artifact it is necessary to have a longer TE value associated with a high TR value (to maintain a high SNR). If a good compromise between TE and TR is not found, to be able to see both lesions and metal markers we need to do different scans with different settings for the two purposes.
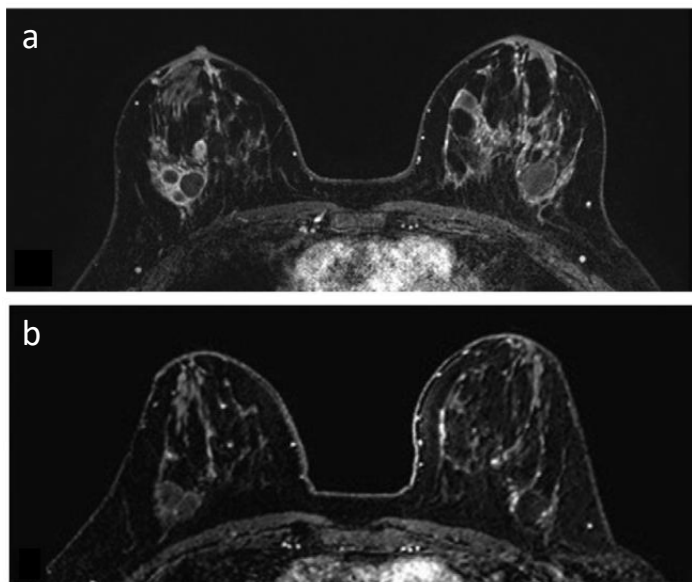

Figure 4. Comparison of a T1 GE 3D axial sequence on 1.5T (a) and 3.0T (b) machines [24].

Injected dynamic 3D sequences are instead useful to locate exactly the lesions as it reconstructs the total breast volume, this facilitates the identification of the region of interest and its characterization. Breast MRI sequences without contrast agent are less utilized because they have a low diagnostic value of T1 and T2 signals. Thanks to the use of medium contrast agent, breast MR highlights the neoangiogenesis of tumoral tissue.

Tumor regions have a higher vascularization than the other tissues, this guarantees a very high contrast absorption which in the image results as a more intense signal. MR images have a high sensitivity but the biggest limitation for this type of acquisition is low specificity which can lead to several false positives [23] [24].

2.2 Dynamic Contrast Enhanced MRI

Dynamic Contrast Enhanced MRI (DCE-MRI) is one of the most important MRI acquisition for the identification of malignant tumor lesions. DCE images provide tumor morphology and contrast kinetics information from which it is possible to obtain a series of physiological parameters showing the behavior between the tumors and adjacent tissues [22]. Cellular density, micro-vascularity permeability and tissue perfusion can be obtained thanks to the use of an appropriate pharmacokinetic model.

DCE is based on the rapid diffusion of a contrast agent, the agent generally used is Gadolinium. The contrast medium is injected through an injector which is loaded with syringes containing 20cc of physiological and 0.2cc x body weight of Gadolinium. Observing the perfusion of Gadolinium, it is possible to obtain useful information for diagnostic purposes. Typical DCE images are acquired before and after the injection of the contrast agent (CA), observing these images we can see how tissue absorb and release the contrast agent over the time [25]. Differently from DCE-CT the variations of MR signal are not linearly correlated with the variation of the contrast concentration. MR images can be acquired using T_2* or T_2 weighting DCE-MRI (known as dynamic susceptibility contrast MRI or DSC-MRI), or T_1 weighting (T_1 weighted DCE-MRI).

Dynamic susceptibility contrast MRI. In DSC-MRI the loss of the signal is related to the change of the contrast agent concentration. To estimate a baseline a series of pre-contrast injection is acquired, the contrast agent is then injected as an intravenous bolus with the auxilium of a pump, followed by a saline flush. The images are acquired in different times so the time-intensity signal can be used to estimate the CA concentration in the tissues. The susceptibility contrast mechanism is related to changes in the local field within the tissue caused by paramagnetic contrast molecules. These variations also influence water molecules away from the contrast, so measurements of apparent CA concentration will be influenced by the local vascular structure. This technique is useful in study changes in grey and white matter because SNR is better than in T1 weighted techniques, furthermore it provides information about size and distribution of vessels. In tumor tissues, an analysis of endothelial permeability is possible, but the change in the signal in the tissues around the contrast medium makes this analysis less reliable. For this application, therefore, it is preferable to use the T1 weighted DCE-MRI technique.

T_1 weighted DCE-MRI. T1 weighted DCE images are a sequence of total volume imaging that is repeated over time. Time scans are acquired for the 5 minutes following the injection of the contrast agent. A T1 measurement is performed before the contrast injection and then it is rapidly repeated several times in the next 10 minutes after intravenous injection of gadolinium. This sequence can be acquired in 3D or 2D: three-dimensional imaging is acquired by applying suitable gradients during image acquisition; 2D imaging, on the other hand, are obtained by means of selective excitation. 3D imaging has a shorter repetition time than the 2D multi-section image and allows to obtain thinner sections because it has a higher intrinsic signal-to-noise ratio. However, a 2D sequence

suffers less from motion and pulsation artifacts. Both sequences can be performed with and without fat suppression.

2.2.1 Functional MRI

From the 3D sequences it is possible to obtain the intensity-time curve and concentration-time curve (TCC). The intensity-time curve (or signal-time curve) is basically the MR signal intensity of a single voxel or a region of interest plotted over the acquisition time point; it provides useful information to evaluate the absorption rate and clearance of gadolinium in the tissues and from this evaluation obtain biomarkers of the tissues vasculature. The rate of contrast uptake in breast lesions is non-linear and differs between malignant and benign lesions as can be seen in Figure 5. This feature is very useful for differential diagnosis. Malignant lesions exhibit stronger and faster contrast absorption than other tissues (type III). In the benign lesions the curve has an increasing continuous progression in all the temporal instants (type I). In cases where the curve presents a plateau (type II) the lesion classification is doubtful [26].
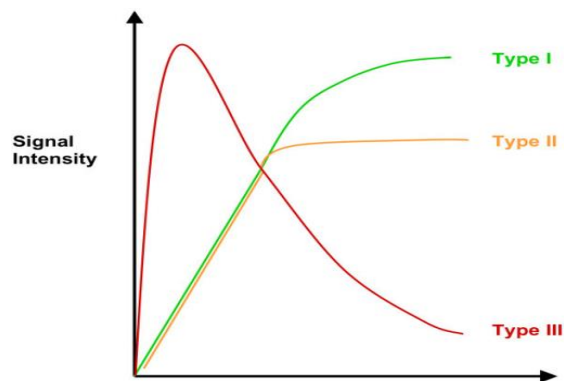

Figure 5. Time-intensity curves for breast lesions [26].

To determine the concentration time curve, time intensity curve and pre-contrast scans are necessary. TCC depend on the relaxation of the CA used and the acquired T1 signal, it represents the relation between the concentration (or dosage) and the time needed to produce an action.
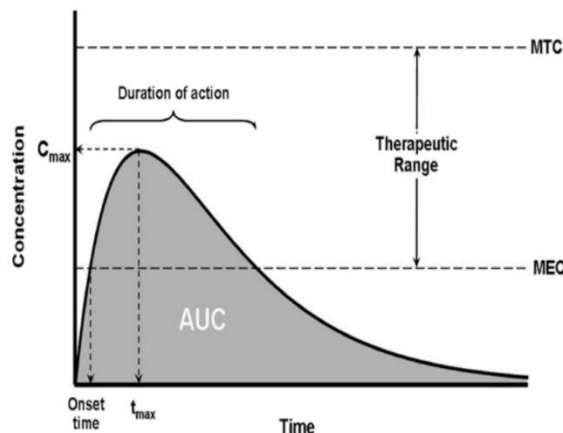

Figure 6. Time concentration curve, AUC is the area under the curve, it represents the number of molecules of CA present and it estimates the release time.

7

TCC is analyzed performing a kinetic model using curve-fitting [27], the accuracy of the curve-fitting techniques is influenced by the temporal resolution, the SNR and by the pharmacokinetic model utilized, whereby the validity of the parametric estimates will be directly influenced by the quality of the data. Although the acquisitions can be optimized, there is still a compromise between temporal resolution, SNR and tissue coverage. The most commonly adopted solution is the choice of a simplified pharmacokinetic model that improves accuracy at the expense of biological specificity [28].

2.3 Data collection (DCE-MRI)

Patients involved in this study were subjected to a Mammary Magnetic Resonance examination by 3T MRI scanner. All patients had breast abnormalities on mammography or sonography, confirmed by cytology and/or micro-biopsy.
10 patients were examined, 5 pre-neoadjuvant therapy and 5 post-treatment. Of these post-treatment patients several scans were available, overall 15. Thanks to post-treatment scans it was possible to evaluate the functioning of the algorithm also for monitoring the effectiveness of the therapy.
All images were provided by Borgo Trento Hospital in Verona.

2.3.1 MRI Protocol

All patients were scanned at 3T scanner (Philips Achieva STx) with a 16-channel breast coil used only for diagnostic purposes. Patients were placed in prone position on the MammoTrak with breasts falling into the appropriate cavities and the arms positioned above the head. The breasts must be "hanging" freely in the coil and they must be free of folds. All scans were made with fat-suppression. The automatic injector of contrast agent was connected via the cannula to a peripheral vein of the patient.
The bed was lifted and introduced into the gantry, the light visor is centered to the middle of the breast and then the patient is completely introduced into the gantry from the feet side [29].
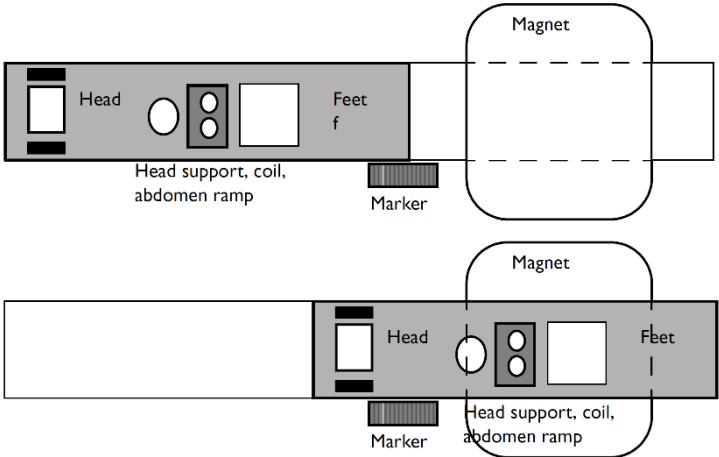

Figure 7. MammoTrak Set-up (upper row). MammoTrak is approached to the gantry until the breast coil is aligned with the isocenter (lower row) [23].

Over the common T1-TSE (TR/TE=400/10ms) and T2-STIR (TR/TE=5000/60ms) sequences, Dynamic contrast enhancement (DCE) were acquired.

This scan includes multiple T1-weighted acquisition before and after injection of gadolinium multihance contrast. 6 scans were acquired every 90 seconds, application of the contrast agent was started after the first scan. 195 slices were acquired per scan, with a total of 195x6=1170 images. TR/TE 4.8/2.4 ms; FOV, 340 mm (RL and AP), 175.5 mm (FH); the dimensions of matrix are 384x384 with voxel size 0.90x0.90x0.90 mm. Total scan duration was around 9 minutes.

Chapter 3

Lesion detection algorithm

The lesion detection pipeline consists of five main steps: image registration, pre-processing, breast region contouring, lesion segmentation and heuristic analysis of the results. The fully automated segmentation algorithm works on each slice separately but in the post-segmentation phase, overall considerations will be made on the whole volume for false positives reduction.

The algorithm was built in Matlab. To have a greater morphological consistency, the images are first registered and then subjected to a preprocessing phase.

Volume slice are 195, for each slice breast region is selected to prevent false positives due to structure such as heart and vessels that are not of clinical interest in this application. On the isolated region we initialize a Level Set algorithm for skin detection followed by a Thinning algorithm for removal of skin contour. Double threshold Region Growing is subsequently applied, after an appropriate thresholds selection, the algorithm recognizes lesions and then segments the contour of the identified region. In the last step, a geometrical evaluation and intensity-based considerations help to reduce the number of false positives.

All these steps are reported in Figure 8, the flowchart represents all phases of the algorithm with the relative results. At the end of the false positives reduction geometric features and texture analysis were calculated both on the single segmented slice and the entire volume.
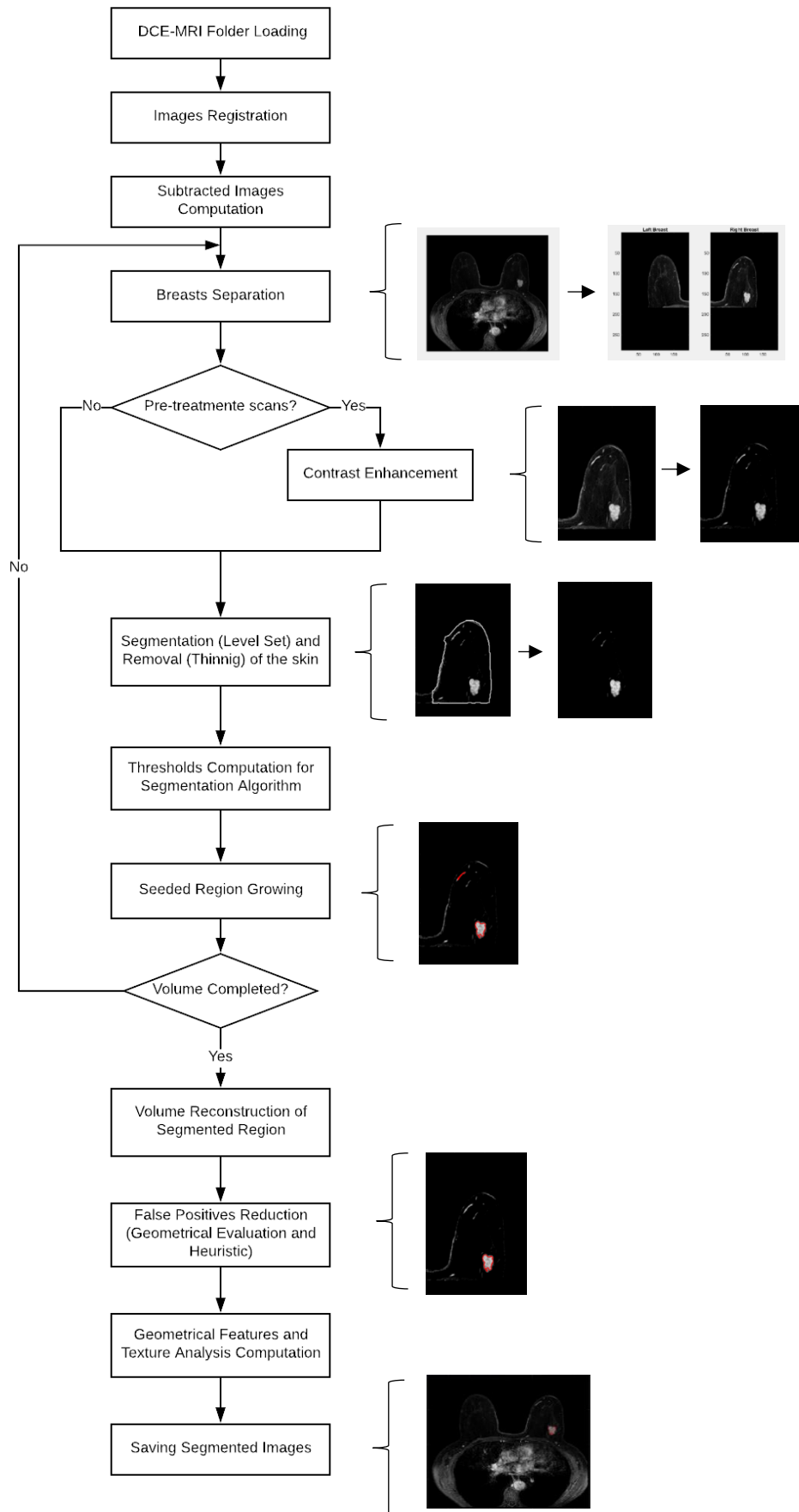
Figure 8. Methodology flowchart.

3.1 Image registration

The first step of the algorithm is the registration of the volumes, the DCE-MRI provided are composed of one pre-contrast injection scan and five scans post-contrast injection. For the image registration the fixed volume is the pre-contrast acquisition and the five subsequent volume are rigidly realigned to the fixed volume.

The rigid realignment function is based on the intensity image distribution, Matlab function *imregconfig* is used to set the configuration parameters for the registration.

PARAMETERS	DEFAULT VALUES	SETTED VALUES
Gradient Tolerance Magnitude	10^{-4}	10^{-4}
Minimum Step Length	10^{-5}	10^{-3}
Maximum Step Length	0.0625	0.1
Maximum Iterations	100	50
Relaxation Factor	0.5	0.5

Table 1. Optimizer metric configuration.

To evaluate the convergence of the results the metric used is the mean square error, the other parameters of the registration optimization are reported in Table 1. To improve the algorithm performances some default values are changed, in this way computational time are lower and even if the results are less performing, this does not affect the effectiveness of the algorithm. Values changed are minimum step length, maximum step length and maximum iterations:

- Minimum Step Length defines how accurate the process must be;
- Maximum Step Length is the maximum stride length;
- Maximum Iterations is the maximum number of iterations the optimizer performs at any pyramid level.

The metric and optimization values are loaded in the *imregister* function which realign the moving volume to the fixed volume. This function builds an image pyramid that has N levels, each level decreases the resolution by a fixed factor.
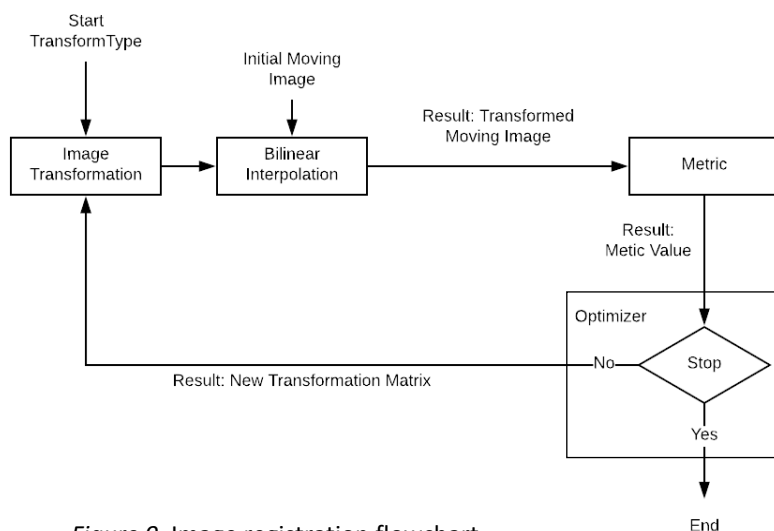

Figure 9. Image registration flowchart.

Starting from the lower resolution step of the pyramid the function run until the Maximum Iterations is reached or until the optimizer converges, the process flowchart is represented in Figure 9. At this point the function restart with the current transformation estimate on the next pyramid level. This process continue until the full original resolution is reached.

3.2 Pre-processing

The algorithm pre-processing consists of several phases, after the loading of the DCE-MRI folder, the uploaded images are processed in order to obtain 195 slices representing the entire volume, containing properties of the different time scans. On the slices thus obtained several steps are applied to obtain the axial image division in two sub-images. Start from this point the algorithm will work separately on each breast. In Figure 10 we can see the steps of the pre-processing phase: after the axial image division in two sub-images a contrast enhancement is applied only if the scans are pre-treatment, later the reason of this distinction will be explained.
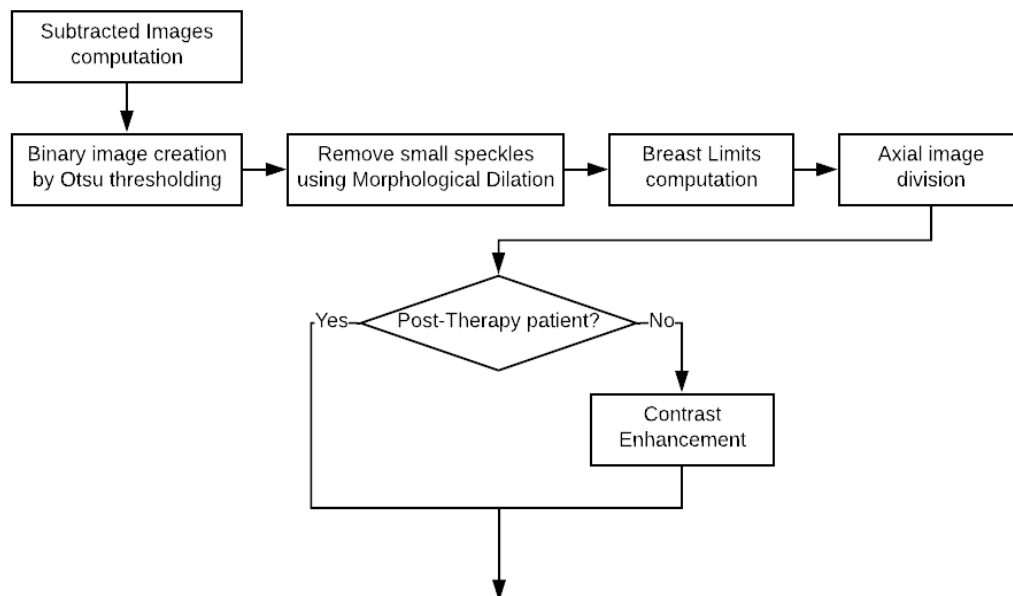

Figure 10. Pre-processing flowchart.

3.2.1 Subtracted images computation

DCE-MRI folder includes 1170 images for the six-time scans, every scan includes 195 images each representative of a slice belonging to the entire breast volume. To better emphasize the contrast perfusion, it was decided to calculate the subtracts of the different scans.
In order to choose the correct combination several tests were made, Figure 11 shows some of the tests carried out, at each scan starting from the first post contrast injection, the pre-contrast scan was subtracted, the result being that the perfused regions remain still bright, the other areas are attenuated. This is a significant advantage for ensuring fewer false positives.
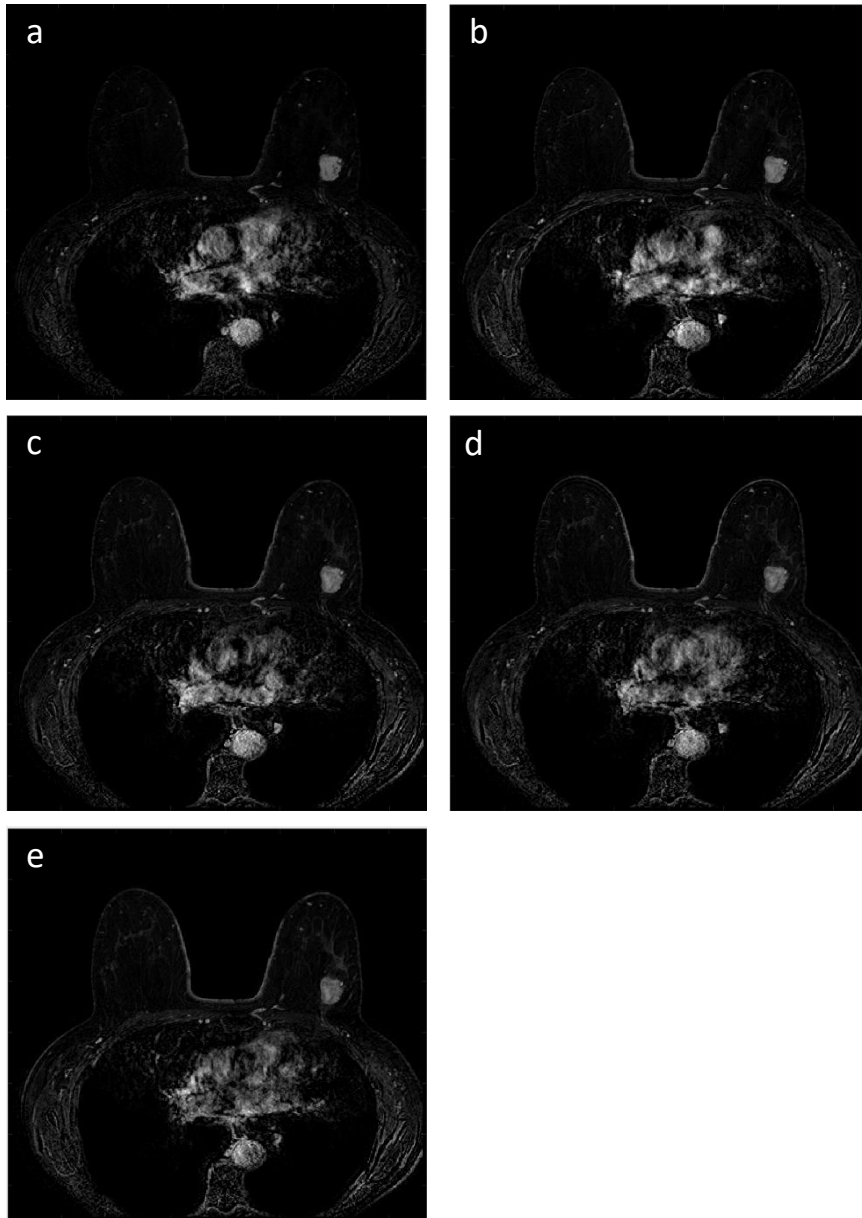
Figure 11. Subtraction example. Considering *pre* the pre-contrast scanning and *post1, post2, post3, post4* and *post5* respectively the first, second, third, fourth and fifth post-contrast scanning, the images can be defined as: (a) post1-pre, (b) post2-pre, (c) post3-pre, (d) post4-pre, (e) post5-pre.

From the examples of Figure 11 it is possible to deduce that the images with a higher intensity are the first two, the third still has good evidence of the lesion but the image has other artefacts for which it is discarded. From a comparison with the clinicians it has been confirmed that the first two post-contrast scans are those of greater clinical interest, this is why at this stage it was decided to consider only the first two.

Evaluating the results obtained with these scans and after having carried out further tests, we found the solution that would optimize the algorithm's performance. The operation consists in the sum of the first two post-contrast images and, to the image obtained we subtract the pre-contrast image:

$$Img\{i\} = images\{i + n_{slice}\} + images\{i + 2 * n_{slice}\} - images\{i\}$$

Img{i} is the current output image, *images{i+n_slice}* and *images{i+2*n_slice}* are respectively the first and the second post-contrast image of the current i-th image, while *images{i}* is the i-th image acquired before contrast injection.

This operation is repeated for each of the 195 images acquired, at the end *Img* will contain the subtracted images of all 195 slices. This aid to emphasize the region more perfused by the contrast agent.
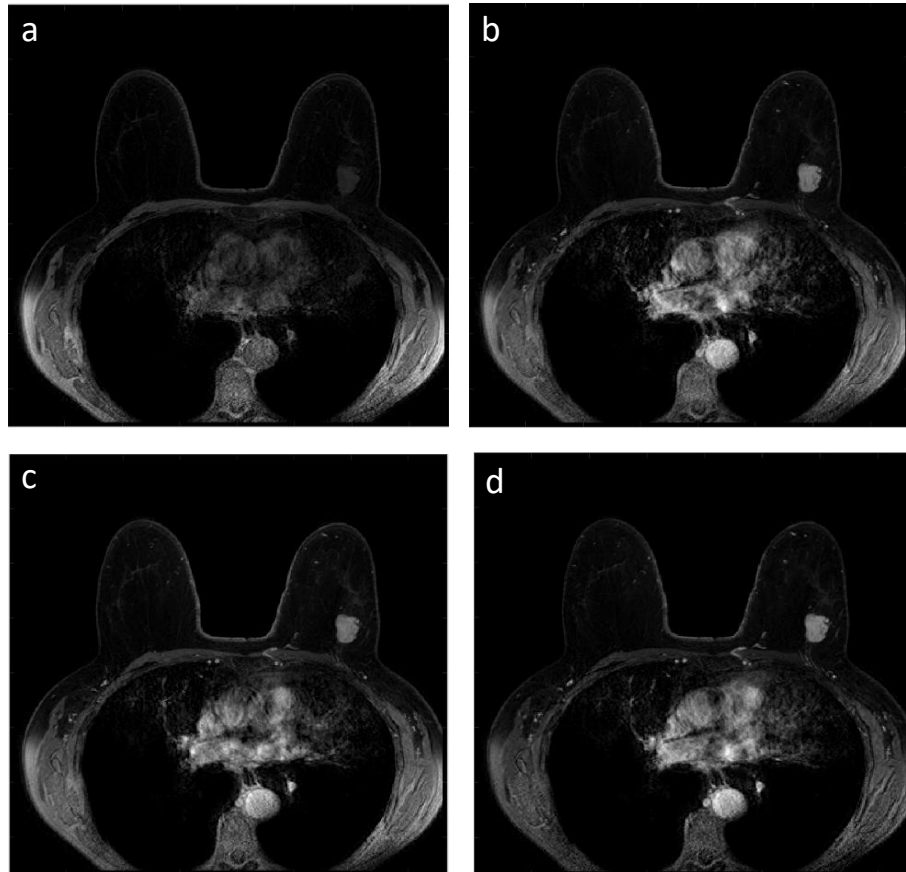

Figure 12. Representation of the slice 23 (patient 3) in the different time scans necessary to calculate the subtracted image. (a) pre-contrast scan, (b) first post-contrast scan, (c) second post-contrast scan, (d) result of the subtraction.

3.2.2 Axial image division in two sub-images

Algorithm works on each breast separately; the division of the image is therefore a fundamental step because it defines the region that the algorithm will explore. A wrong selection of the region would inevitably lead to a wrong segmentation.

To select only the breast region, several steps have been performed. First a binary mask is created; for the discrimination of the object from the background Otsu threshold is selected, the Matlab *adapttresh* function is implemented with a sensitivity value equal to 0.4.
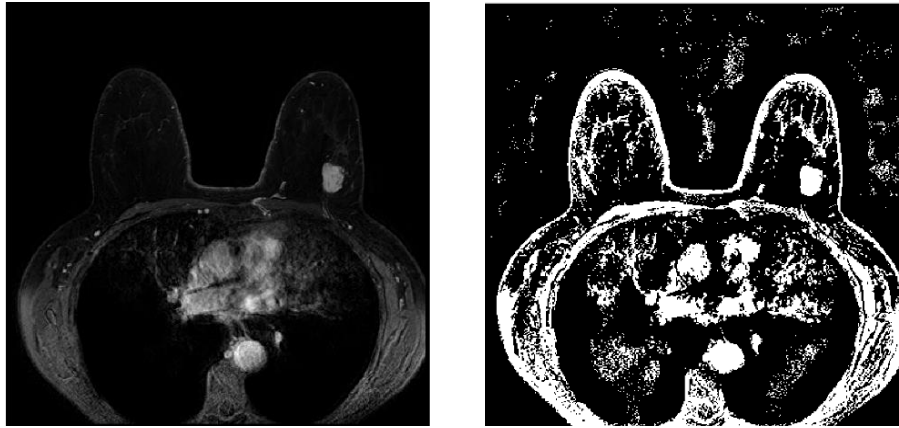
Figure 13. Original gray scale image (left) and binary mask (right).

Otsu thresholding generate white area in the background because of the intensity noise in the image, to delete this artifact a morphological operator is used. One dilatation is applied with a structural element 'disk' of radius 3. Then the biggest area is selected with the Matlab function *bwareafilt* (Figure 14).

Figure 14. Result of morphological operator (left), result of biggest area selection (right).

To estimate the breast location the most anterior point of the breast is defined as the upper limit, and the deepest point between the two breast is the lower limit. To ensure that no tumor lesion is lost near the ribs, a safety margin, of approximately 20 pixels, is added to the lower limit.

For the initial contour of the level set, as we will see in paragraph 3.3.1, the external limits (left limit and right limit) of the breasts will also be useful (Figure 15).
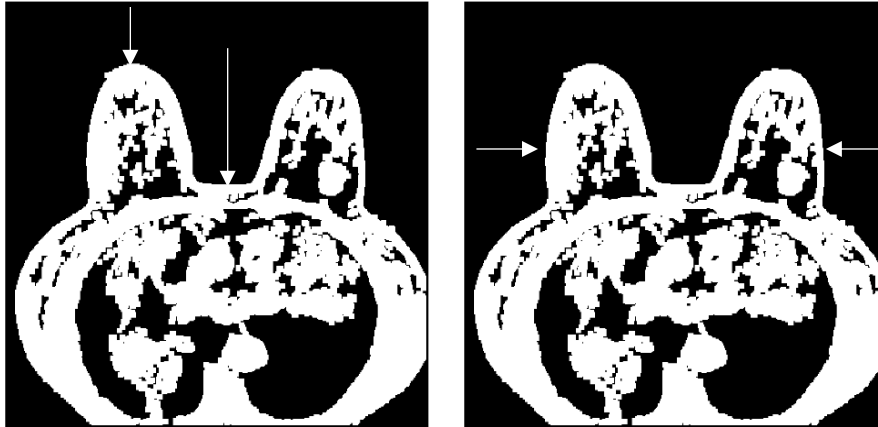
Figure 15. Identification of upper and lower limit (left) and left and right limit of the breast (right), shown by arrows.

In this way we have localized the position of the two breast, and then the axial image division in two sub-images is implemented (Figure 16).
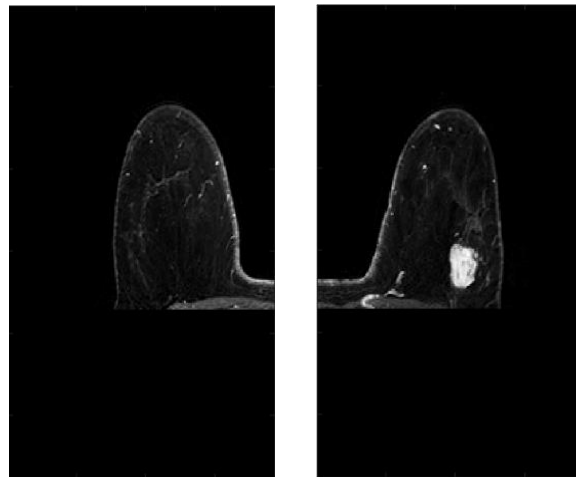

Figure 16. Axial image division after breast localization.

Matrix dimension is 288x193, this value is fixed for all slices because to correctly reconstruct the volumes it is necessary to have all the images of the same size.

3.2.3 Contrast enhancement

To emphasize the region of interest (ROI), a contrast enhancement is implemented. The variation of contrast is useful because the bright objects became highly different from the background, to do that we have to change the intensity of each pixel. The reference value for the brightness change, calculated for left and right breast separately, is the Luminance L:

$$L = \frac{IOD}{mxn} = \frac{\sum pixel}{mxn}$$
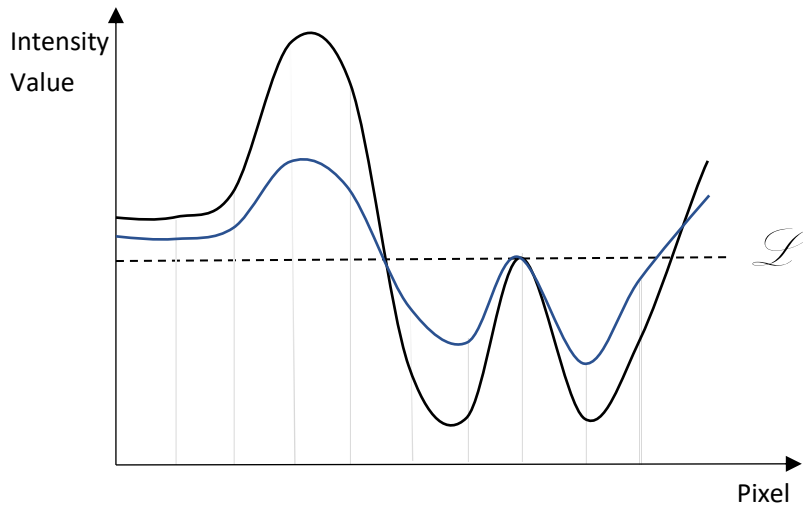
Figure 17. Curve representing the variation of contrast.

In Figure 17 the horizontal line is the luminance value, the curve blue represents pixels intensity of the original image, the curve black represents the intensity profile of the same pixels after the variation of the contrast.

All intensity values higher than the luminance is increased, those with a lower value are attenuated. The variation of the intensity value is proportional to the distance from the luminance, pixels with intensity value very distant from the luminance will have a higher variation. Several tests were carried out to select the percentage value for the contrast variation that would provide the best results.
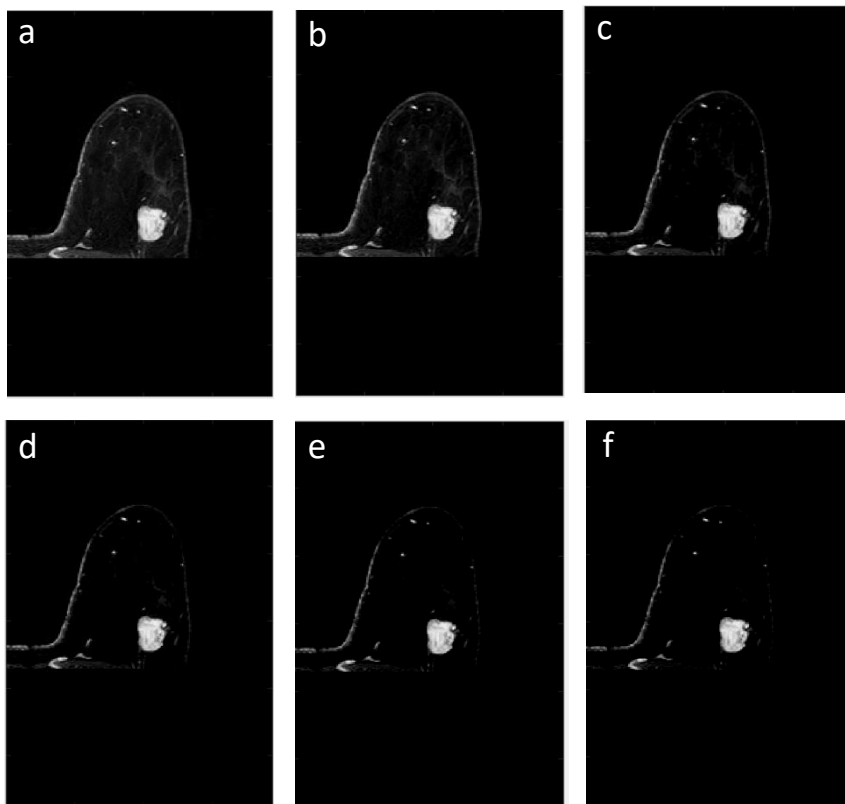

Figure 18. Results of the different percentage variations of the contrast. (a) Original image, (b) 10%, (c) 30%, (d) 50%, (e) 70%, (f) 90% of intensity pixel variation respect to the luminance distance.

Figure 18 shown the effects of the contrast enhancement with different percentages of intensity pixels variation; applying a variation of 10% or 30%, several elements in the image are not sufficiently attenuated so they could lead to incorrect segmentations. Between the 50% and the 90% of variation, from the observation of the images in Figure 18, there are no big differences; to choose the most appropriate value, several tests have been carried out iterating the algorithm on images with different percentage values. From these tests it was observed that with a more accentuated variation of the contrast a greater selectivity was guaranteed in the choice of the seed that in other cases led to a wrong segmentation (Figure 19).
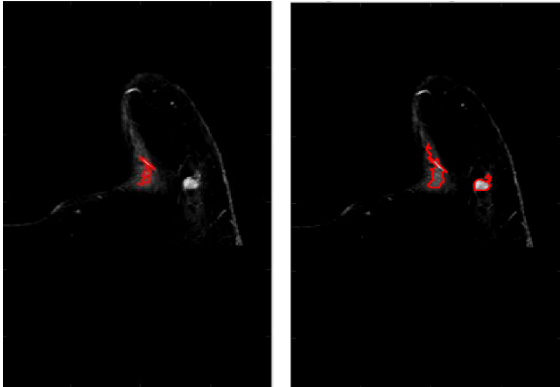
Figure 19. Segmentation result with contrast variation of 50% (left) and variation of 70% (right).

This means that a greater contrast more emphasizes tumor regions than other noise areas, allowing the algorithm to select more specifically the threshold for lesions detection. For this reason, the pixel intensity is increased or attenuated of the 70% of its distance from the luminance, based on its original intensity value.
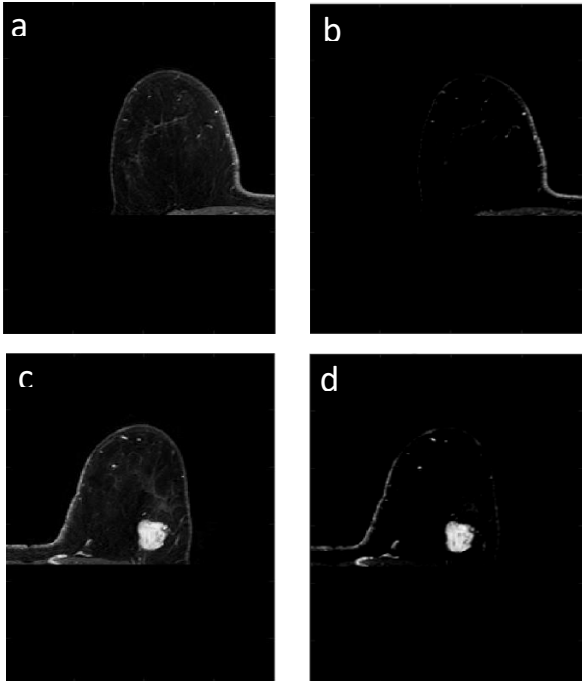
Figure 20. Contrast enhancement. (a, c) Original gray scale intensity for the left and right breast respectively, (b, d) left and right breast after contrast

19

Contrast enhancement provides significant advantages when the lesions are brighter and more defined than the background, this property is not always respected by the scans carried out after neoadjuvant therapy. For this reason, to avoid missing identification of tumor regions, in post-treatment scans the contrast is not changed and the segmentation algorithm work on the original images.

3.3 Breast skin removal

Breast skin has intensity value comparable to those of tumor lesions, the purpose of this step is to identify the breast contour and eliminate the skin. This phase is necessary to reduce the possibility of error in the selection of the seed and it also decreases the number of false positives. For breast skin detection a Level Set algorithm has been implemented followed by a Thinning algorithm to delete the breast skin border. Image resulting from these processes includes only the internal region of the breast in which the thresholds for the lesion contouring algorithm will be chosen.

3.3.1 Breast skin detection (Level Set)

Level set method is a geometric deformable model, this technique can conform numerical computations without the need to parameterize the objects to be contoured. To detect the breast contour, we use a bidimensional level set formulation. The initial contour represented by the zero-level set is defined as $C(t) = \{(x, y) \mid \phi(t, x, y) = 0\}$ of a level set function $\phi(x, y, t)$. Each point of the level set function has a value corresponding to the Euclidean distance from the boundary point closest, the external points having the greatest distance are the vertices, the internal point having the greatest distance is the center. The representation of the level set in three dimensions is represented in Figure 21, the points on the contour have distance value equal to zero.
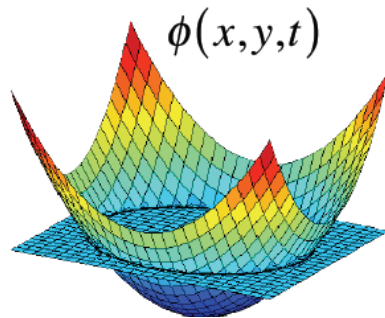
Figure 21. Level set functional evolution.

The level set equation is the following:

$$\frac{\partial \phi}{\partial t} + F|\nabla \phi| = 0$$

The function F is the speed function and depends on the image and the level set function ϕ, this term is the one that iteratively moves the boundary towards the object. In traditional level set function, ϕ can develop irregular shapes that induce to a wrong contouring, to solve this problem a re-initialization of the function is periodically applied during the evolution, but the re-initialization process can be complicated and sometimes it can also deviate from the desired result. In this work we used a variational formulation of a level

set evolution without Re-initialization, as proposed by Chunming et al. [30]. This method forces the active contours to be near to a defined distance function, in this way the re-initialization process is not necessary.

The energetic function, which move the active contour towards the region to be outlined, is a combination of an internal energy term ($P(\phi)$) and an external energy term ($\varepsilon_m(\phi)$):

$$\varepsilon(\emptyset) = \mu P(\emptyset) + \varepsilon_{g,\lambda,v}(\emptyset)$$

The internal energy term penalizes the deviation of ϕ, it is defined as:

$$P(\phi) = \mu \left[\Delta\phi - div\left(\frac{\nabla\phi}{|\nabla\phi|}\right)\right]$$

Where $\mu > 0$ is a parameter that regulates the effect of penalizing the deviation of ϕ and Δ is the Laplacian operator. The external energy term otherwise moves the zero-level set towards the object contour, it is composed by two terms, one that computes the length of the zero-level curve and the other representing the weighted area. These terms can be expressed as follows:

$$\varepsilon_{g,\lambda,v}(\emptyset) = \lambda\delta(\phi)div\left(g\frac{\nabla\phi}{|\nabla\phi|}\right) + vg\delta(\phi)$$

Where $\lambda>0$ and v are constant (v can be positive or negative depending on where the zero-level set is positioned relative to the object), δ is the delta di Dirac function and g is the edge indicator function:

$$g = \frac{1}{1 + |\nabla G_\sigma * I|^2}$$

With I image and G_σ the Gaussian kernel whit a standard deviation σ. The formulation for delta di Dirac function is:

$$\delta_\varepsilon(x) = \begin{cases} 0 & |x| > \varepsilon \\ \frac{1}{2\varepsilon}[1 + \cos\left(\frac{\pi x}{\varepsilon}\right), & |x| \leq \varepsilon \end{cases}$$

Algorithm iterates a certain number of times (N_iter) as long as the curve does not reach the convergence. The equation representing the update of the level set curve is the following:

$$\emptyset = \emptyset_0 + time_{step} * \varepsilon_\emptyset$$

Where ϕ is the new level set function, ϕ_0 is the zero-level set function (previous iteration) and ε_ϕ is the energy contribution. Time step is a multiplicative coefficient that increases the variation for each iteration, in this way it can reduce the number of iterations.
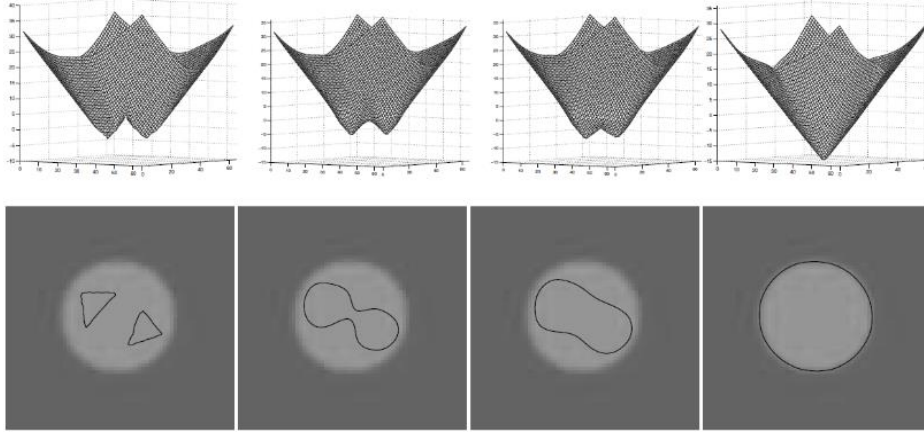
Figure 22. Level set evolution: evolution of level set function ɸ (Row1) and evolution of the corresponding zero-level set curve (Row2). The first column is the algorithm initialization, the fourth column is the converged result [30].

In the listed formulations there are a series of numerical parameters (constants) that must be set. Some of these parameters have been chosen according to the criteria of other applications on MRI images, while others have been chosen specifically for the images used in this application.

PARAMETERS	VALUES
μ	0.04
λ	5
ν	1.5
ε	1.5
Time step	5
N_iter	80
σ	1.5

Table 2. Level set parameters setting.

Values μ, λ, ν and ε have been selected by others study [31]; time step, n_iter and σ instead they have been chosen to adapt them better to our needs. Varying these parameters, the algorithm's performances change; several tests have been performed, with different combination of these values. Increasing too much the σ value, with an equal number of iterations, the level set did not correctly distinguish between outside and inside the breast, the most appropriate value found is 1.5. Once σ has been set, other tests have been carried out to choose the most appropriate number of iterations, the combination that led to the best results is time step equal to 5 and n_iter equal to 300.

In this work computational times are very important, so to improve the speed of level set method without reducing its performance, the zero-level set is initialized near the breast, to do that we use upper and lower limit of the breast and we also get the lateral limits of the breast previously obtained (Paragraph 3.2.2), in this way only 80 iterations are sufficient to obtain a correct contouring of the region.
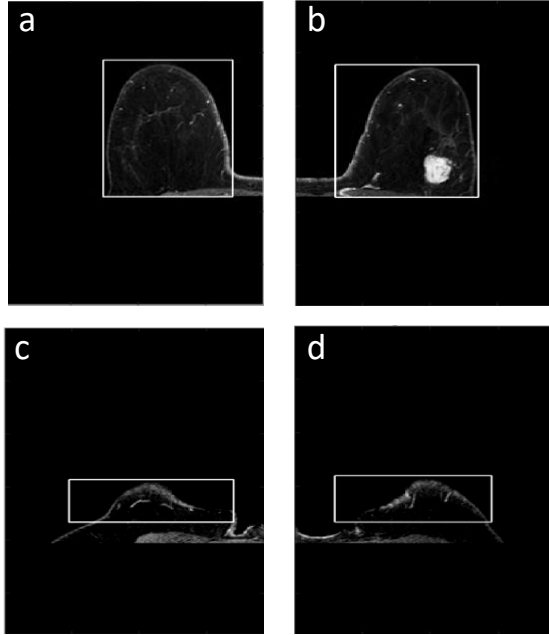
Figure 23. Examples of zero-level set initialization in two different slices. (a, b) Patient 3, slice 23 respectively left and right breast. (c, d) Patient 3, slice 74 left and right breast.

The first zero-level set is created by constructing an initial mask of the same size as the original image where the pixels within the initial outline have the same negative value, the external ones have the same positive value.

In Figure 24 we can see the results of the Level Set contouring.
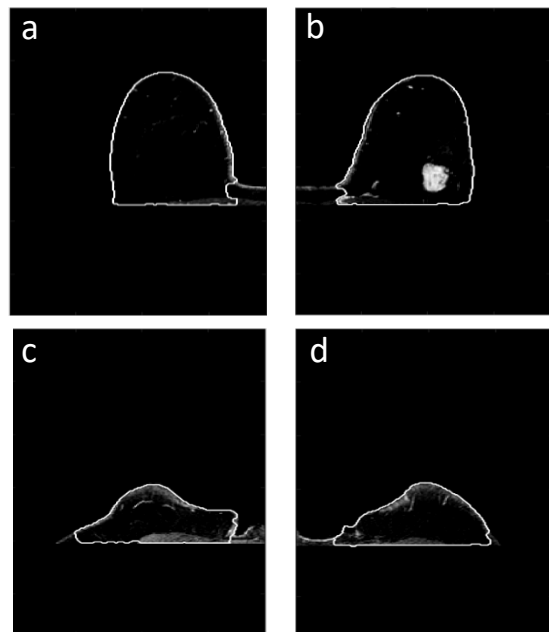

Figure 24. Examples of level set segmentations of different slices. (a, b) Patient 3, slice 23 respectively left and right breast. (c, d) Patient 3, slice 74 left and right breast.

3.3.2 Breast skin elimination (Thinning)

After skin detection, the breast contour is deleted with a morphological thinning operator. Thinning is a topological skeleton which erodes pixels from the boundary, comparing the pixel with its neighborhood.

This technique iteratively eliminates the pixels of the object contour to reduce it without altering its morphology. Thinning operator works on binary mask, to decide if the current pixel should be deleted an 3x3 neighborhood is considered. The conditions to be respected are divided into two iterations:

1. Pixel p is deleted if and only if the first three conditions shown below are all satisfied.
2. Pixel p is deleted if the first two and fourth conditions are all satisfied.

First condition:

$$X_H(p) = 1$$

Where

$$X_H(p) = \sum_{i=1}^{4} b_i$$

$$b_i = \begin{cases} 1, & \text{if } x_{2i-1} = 0 \text{ and } (x_{2i} = 1 \text{ or } x_{2i+1} = 1) \\ 0, & \text{otherwise} \end{cases}$$

x_i are all values of the eight neighbors of p.

Second condition:

$$2 \leq \min\{n_1(p), n_2(p)\} \leq 3$$

Where

$$n_1(p) = \sum_{k=1}^{4} x_{2k-1} V x_{2k}$$

$$n_2(p) = \sum_{k=1}^{4} x_{2k} V x_{2k+1}$$

Third condition:

$$(x_2 V x_3 V \overline{x_8}) \wedge x_1 = 0$$

Forth condition:

$$(x_6 V x_7 V \overline{x_4}) \wedge x_5 = 0$$

The two iterations just listed constitute a single iteration of the thinning algorithm. The Matlab *bwmorph* function, which use the algorithm specified above, is used to remove breast skin.

The thinning algorithm works on binary masks, therefore starting from the contour obtained from the level set method the binary masks are obtained, and different tests are carried out in order to be able to select the number of times the thinning has to be repeated (N_{Th}).

$N_{Th}=11$ is the chosen iteration number that allows the algorithm to remove the appropriate amount of pixel which corresponds to the thickness of the breast skin.
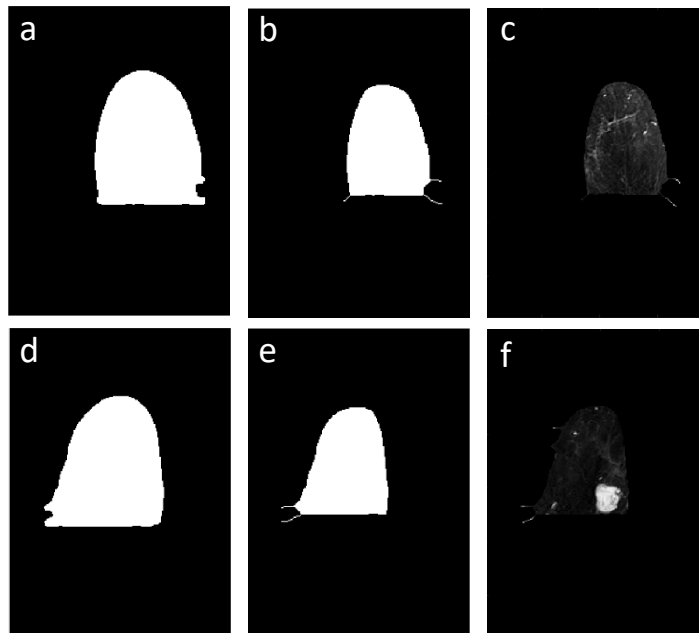
Figure 25. Thinning algorithm results. First row shows the left breast results, and second row is the right breast. (a, d) Binary mask of the level set contour, (b, e) thinning algorithm result, (c, f) original gray scale image after thinning.

Thinning method results have some remaining extensions shown in the red circles (Figure 26) which can lead to wrong segmentations, to avoid this problem a further morphological operator was applied. An erosion operator was applied to the image after the thinning, the structural element used is a 'sphere' of radius 1.
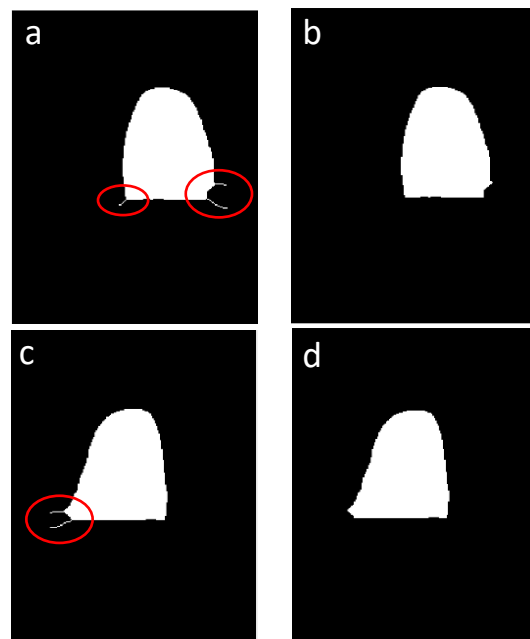
Figure 26. (a, c) Left and right breast respectively. (b, d) Erosion operator results for the two breasts.

The binary image is now reconverted into the original gray scale representation, Figure 27 shows the final result of the breast skin removal.
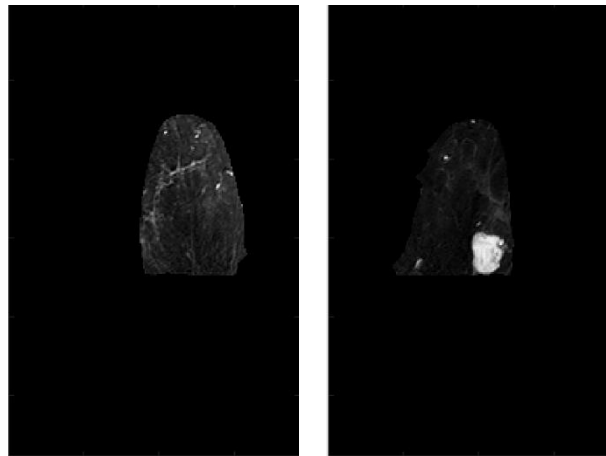
Figure 27. Final gray scale image after thinning (left and right).

3.4 Lesion segmentation algorithm

In this work, the lesion segmentation algorithm chosen is the Seeded Region Growing (SRG). This method is a morphological technique which contours the region maintaining a morphological coherence. The method starts from an initial seed and then SRG begins to grow up, the boundary is defined by a second threshold that distinguishes the object from the background. Generally, these thresholds are set manually, in our case an automatic algorithm for threshold selection has been implemented.
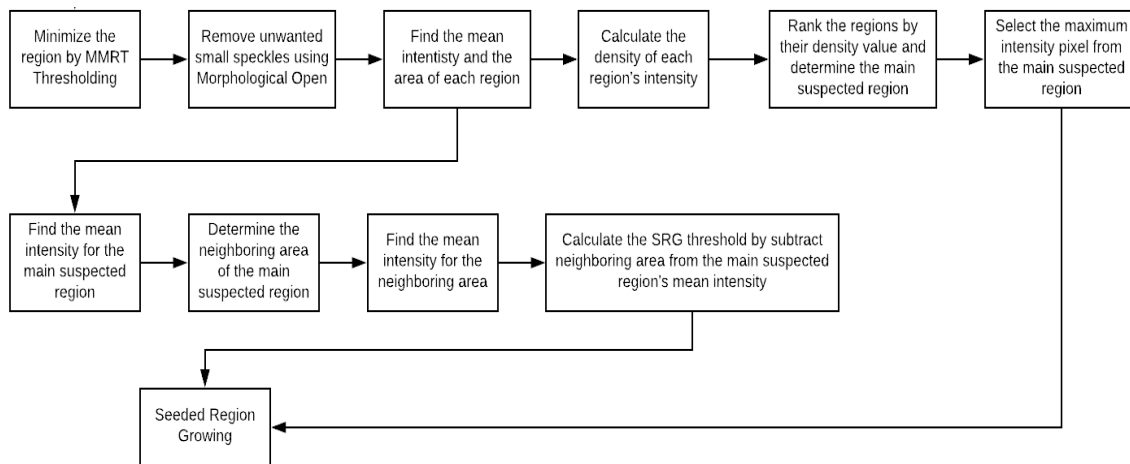
Figure 28. Lesion segmentation algorithm flowchart.

3.4.1 Automatic thresholds selection

The automatic threshold selection includes two main phases, a Seed selection that defines the starting point of the segmentation algorithm (maximum pixel intensity) and the choice of SRG threshold that determines the minimum intensity of pixels belonging to the object, the threshold selection is made independently for each breast.

26

The Seed selection includes 3 main steps:

1. For the selection of a suspected region, a binary mask has been created thanks the Mean Maximum Row Thresholding algorithm (MMRT). This method searches for the maximum value in each row, then a sum of these values is calculated. The MMRT is obtained dividing the sum by the number of rows of the image:

$$MMRT = \frac{\sum_{i=0}^{N} M_i}{N}$$

Where i is the index row of the image, N the total number of rows and M_i is the maximum intensity value of the row i.

To have a more specific discrimination of the suspected region, in this work MMRT is calculated dividing the sum of the rows maximum by the number of rows whose maximum is a non-null value. The calculated threshold is therefore
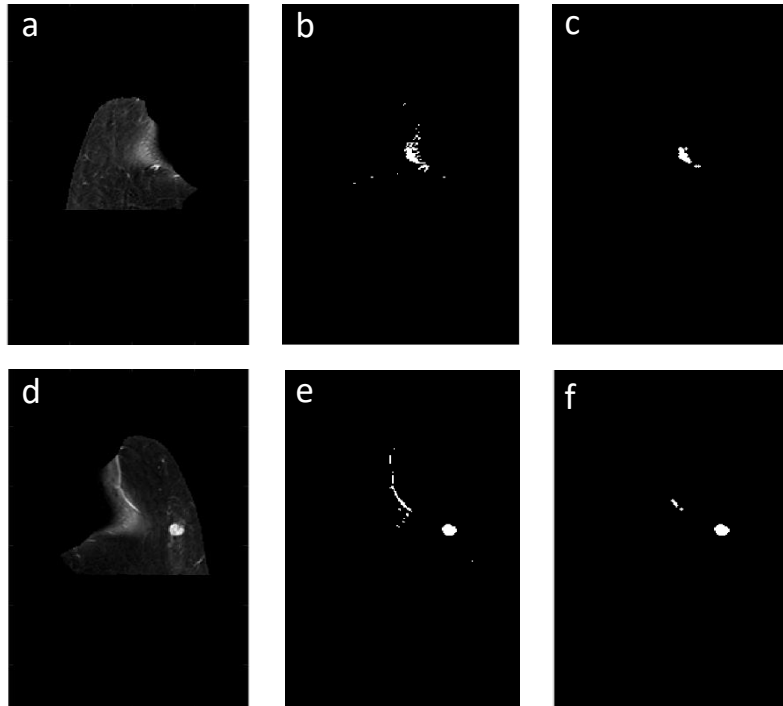
Figure 29. (a, d) Left and right breast original gray scale image after thinning. (b, e) Left and right breast binary mask using MMRT threshold. (c, f) Left and right binary mask after morphological open.

used to create the binary mask using the Matlab function *imbinarize*, pixels with intensity value below MMRT belong to the black region, pixels with the greatest intensity are the white region. The small traces of noise that do not belong to the suspect regions are removed by the application of a morphological open operation (erosion followed by dilation), applied only once with a structural element 'disk' of radius 1 (Figure 29).

2. From the binary mask obtained at step 1, the original gray scale image is extracted multiplying the binary image with the original image matrix. For each suspected region in the image two value has been calculated: mean intensity value of pixels and the area of the region (area is the number of the pixels of the region). From these values, the region's density is calculated dividing the area of each region by the corresponding Mean Intensity value:

$$Region's\ Density = \frac{Area}{Mean\ Intensity}$$

3. Among the regions obtained the one corresponding to the higher density value is chosen as a suspect region (SR), because the tumor region has the highest intensity area among other regions. In SR we will select the Seed value, it is chosen as the maximum intensity value pixel of the region selected.

The selection of SRG threshold is based on an estimated threshold value, it includes 3 main steps:

1. For the SR selected in the previous phase we find the mean intensity value ($MeanInts_{SR}$) in the original gray scale image.
2. The neighboring area of the SR ($Neighboring_{Area}$) is isolated from the unwanted regions like background, breast skin and SR itself. For this region we find the mean intensity value ($MeanInts_{NA}$).
3. Then the SRG threshold has been calculates as the difference between the $MeanInts_{SR}$ and $MeanInts_{NA}$:

$$SRG_{Thr} = MeanInts_{SR} - MeanInts_{NA}$$

3.4.2 Seeded Region Growing

Region growing is part of the morphological operators because it can recognize and contour a homogeneous region of the image. It differs from the classical morphological operators because it can outline even regions that do not have a known geometric shape. This method maintains morphological consistency, it considers the object under examination as a closed object surrounded by other elements that are not the object.

The Seeded Region Growing is an iterative method, it starts from an initial seed and then grow up recognizing all the points belonging to the region. To do this a structural element is defined (exploration region), made from adjacent or connected points to the point under examination. Starting from the seed point the algorithm explore the connected pixels, if
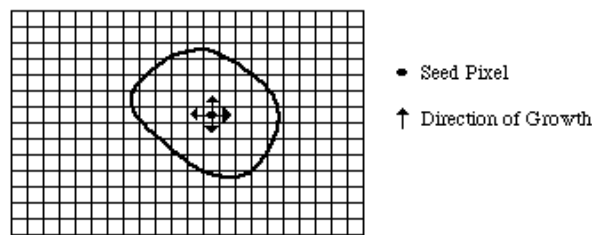

(a) Start of Growing a Region

- Seed Pixel
↑ Direction of Growth
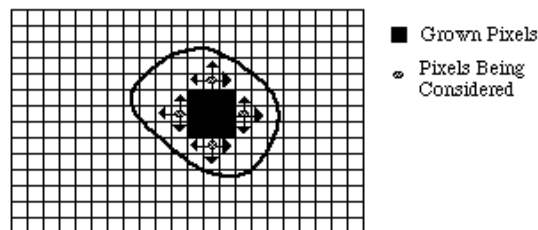
(b) Growing Process After a Few Iterations

■ Grown Pixels
∞ Pixels Being Considered

Figure 30. Region Growing operation.

their value is greater than the SRG threshold, they are joined to the starting point otherwise they are ignored.

Figure 30 shown the intuitive operation of the region growing: from an initial point, the neighbors are explored to evaluate if the near pixels belong to the region. In this example case a 4-connected array was chosen, as the pixels are added to the region their neighborhood should also be explored. These operations are repeated until the entire region has been explored. This method is independent from the initialization, choosing different seeds the result does not change; provided that the seed is inside the region, this variation can affect only the number of iterations.

The algorithm implemented is the double threshold region growing, one threshold is used to identify the seeds, the other one is used for the region propagation. One of the most important step is to choose the seed inside the region to contour, if this condition is not respected the algorithm identifies something in the background that does not belong to the object. For this reason, the seed selection must to be restrictive, therefore in the selection of the seed we have chosen the seed as maximum intensity value of the suspected region selected. If we use the same seed threshold for the region propagation it doesn't work because it is too restrictive, so we need an SRG threshold for the propagation less than the seed threshold. SRG threshold ensures that the pixel incorporated in the region do not belong to the background.

The algorithm stars with the creation of an initial toProcess vector which contains the initial Seed, for each pixel in the vector toProcess the neighbor is explored. If the pixel intensity is higher than the SRG threshold then the pixel is inserted into the toProcess vector and it will be subsequently processed, otherwise the pixel is discarded. The algorithm reiterates as long as the toProcess vector is not empty which means that all the pixels in the neighborhood do not belong to the explored region.
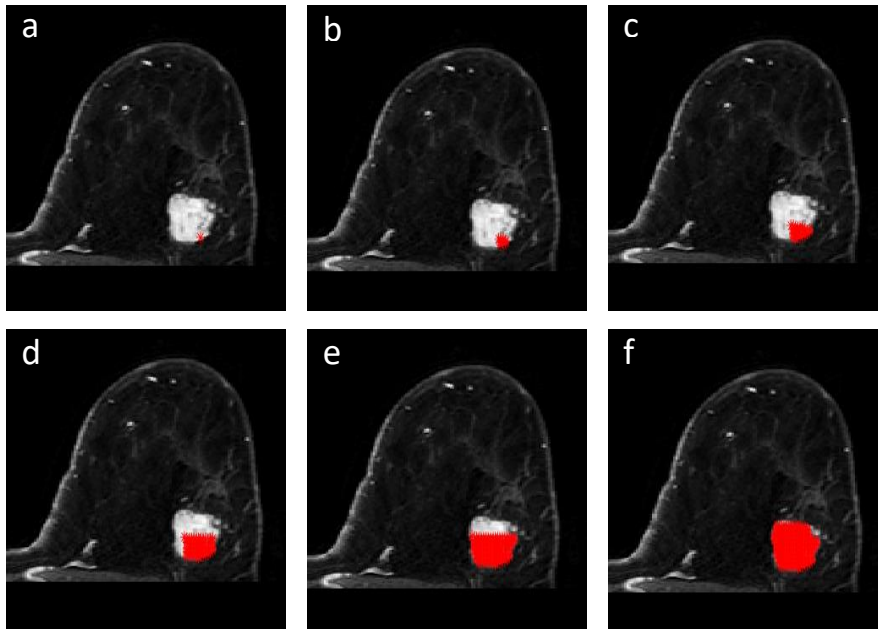

Figure 31. Application of the region growing algorithm. Starting from the initial seed (a) gradually the points joined to the region increase up, until they cover the entire region (f).

Sometimes, pixels in the region do not respect the SRG threshold, so there may be holes in the area. Therefore, we use the Matlab function *imfill* that fills all the holes in the contoured area so that we can only select the external contour (Figure 32).
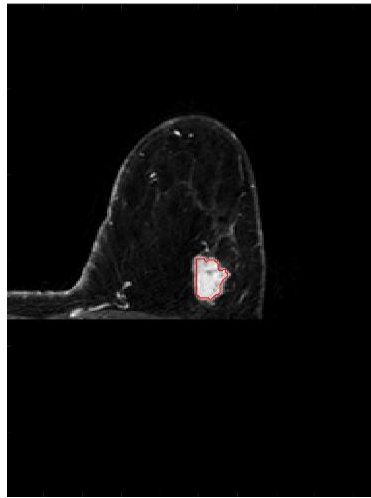
Figure 32. Result of the Seeded
Region Growing.

As alternative to the region growing, a level set algorithm was tested. To be able to automatically discriminate the background, the skin of the breast and the tumor tissues, a 4-phase level set was implemented, each phase ranking one of the previously listed elements, the fourth phase (C_{02}) includes the misclassifications elements that do not belong to any of the other three phases. The logic behind the four-phase level set is the same as for the two-phase level set seen in the paragraph 3.3.1, the only difference is that unlike what happened with the two-phase level set, we can now recognize more colors in the image. The first contour initialization is represented in Figure 33.
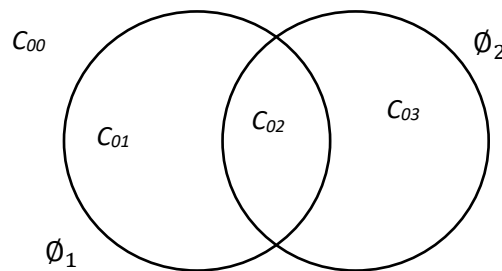
Figure 33. Four phase Level Set. $\emptyset_1$ and $\emptyset_2$ are the
two level set initialization. C_{00}, C_{01}, C_{02} and C_{03} are the
four phases.

All previously applied equations are simply split, the new formulation is the following:

$$\varepsilon(\emptyset) = \mu_1 P(\emptyset_1) + \mu_2 P(\emptyset_2) + \varepsilon_{(g,\lambda,v)}(\emptyset_1) + \varepsilon_{(g,\lambda,v)}(\emptyset_2)$$

The extensive formulation is:

$$\varepsilon(\emptyset) = \mu_1 \left[\Delta\phi_1 - div\left(\frac{\nabla\phi_1}{|\nabla\phi_1|}\right) \right] + \mu_2 \left[\Delta\phi_2 - div\left(\frac{\nabla\phi_2}{|\nabla\phi_2|}\right) \right] + \lambda_1\delta(\phi_1)div\left(g\frac{\nabla\phi_1}{|\nabla\phi_1|}\right)$$
$$+ \lambda_2\delta(\phi_2)div\left(g\frac{\nabla\phi_2}{|\nabla\phi_2|}\right) + v_1 g\delta(\phi_1) + v_2 g\delta(\phi_2)$$

Several test are done to evaluate the performances of the two algorithms. Overall, the results can be considered comparable, but in a careful analysis it was possible to observe different aspects that led to the choice of the region growing rather than the level set:

- The four-phase level set formulation has a double complexity rather than the two-phase level set, the parameters that must be set are doubled so balancing them becomes more complicated.
- Computational time of the level set is longer than the region growing, there is a difference of about 5 seconds for each slice which leads to a total delay of about 16 minutes.
- Number of false positives is greater in the level set, this leads to a further processing time increasing; time increase in a range that varies between 5 and 10 additional minutes, this variation is related to the artifacts in the images.

3.5 Volume reconstruction

The segmentation algorithm works on each slice individually, this means that there is no relationship between segmentations in consecutive slices. This aspect does not affect the ability of the algorithm to segment areas considered suspected regions but certainly by creating a relationship between the slices it is possible to obtain useful information for the discrimination of erroneous segmentation. The volume reconstruction is also used to provide a parametric analysis of the regions of interest, it is helpful for radiologist to obtain useful information for tumor diagnosis.

For these purposes, a function that allows to reconstruct the volumes of each segmented area has been created. The *Volume_Reconstruction* function is applied when the segmentation algorithm has finished contouring all 195 slices, it works on binary images of the segmented regions, so the first step of the function is the creation of a cell vector containing a mask for each slice, the background is black and the segmented region white. This function explores all the masks previously created individually, the *bwlabel* Matlab function is used to create the black and white mask of each segmented area alone, if the mask under analysis is the first it is inserted directly into the vector containing the volumes otherwise checks are made to verify that the regions belong to an existing volume. To be added to the volume made, the segmented region must respect two conditions:

1. the region must intersect with the last slice of the volume at least 30% of the length of the largest area between the two compared,
2. the slice is considered as belonging to the volume only if the slice is adjacent to the last slice of the volume.

If these conditions are not respected, a new volume is initialized.

At the end of all checks a cell vector will be obtained with cells containing the binary mask of the segmented volumes. The reconstructed volumes that extend only on two slices are removed as they are generally associated with noise in the image.

3.6 False positives reduction

One of the limitations of mammary magnetic resonance imaging is the low specificity that can lead to a high number of false positives. For this reason, a correction function is implemented at the end of segmented volumes reconstruction. This correction consists of two main evaluations: a first consideration is made on the geometry of the lesion, the second one is a heuristic evaluation of the results. Geometrical considerations are not very restrictive because the shape variability of the lesion is very high, so it is difficult to create a discriminating criterion that encloses all the variability. For this reason, a heuristic evaluation is added to the geometric criterion to discriminate further wrong segmentations. Heuristic is based on the observation of the wash-in and wash-out curves which provides information on tissue permeability.
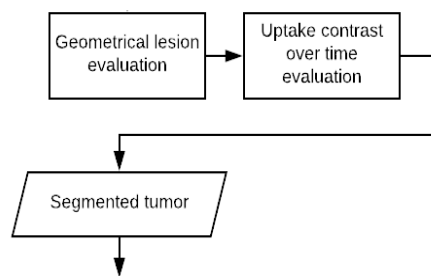

Figure 34. False positives reduction flowchart.

3.6.1 Geometrical selection

The main objective of geometric correction is to discriminate vessels from lesions as they have intensity values comparable to those of suspect regions. The criterion is based on the evaluation of the shape of the segmented region, it is evident that the vessels have an elongated shape almost cylindrical in contrast to the lesions whose shape is regular or irregular but, in any case, almost circular. The evaluation is done both on a single slice and on the whole volume, for small segmentations of vessels the criterion on a single slice is more discriminating than with considerations on the whole volume. For longer vessels, however, the single slice criterion is not sufficiently selective because longer vessels have a greater thickness than the smaller ones and adapting the criterion on a single slice to these vessels would led to a wrong classification of some small tumor lesions. Even if one of the implemented criteria considers the geometry of the segmentation on a single slice, the elimination of the contour remains however linked to the entire volume, we will explain the considerations made below.

It has been observed that the wrong vessel segmentations have a small distance between the two longer sides, the implemented criterion counts the number of contour points that are two pixels away from the opposite side, this verification is made on each slice belonging to the volume and then an overall check on the volume is made to decide if the segmentation should be discarded. There are two conditions:

1. Single slice: more than 31% of the contour pixels are distant from the opposite side less than 2 pixels
2. Whole volume: more than 60% of the slices belonging to the volume respect the condition of point 1.

If these conditions are respected, the contoured volume is classified as a vessel and then discarded. Some examples of this case are represented in Figure 35.
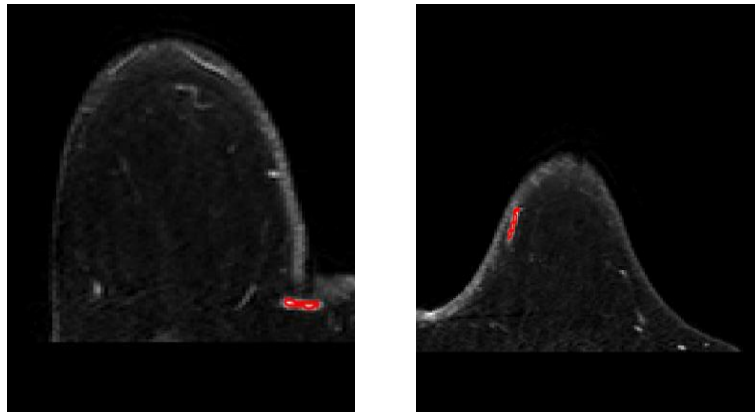

Figure 35. Examples of small vessels segmentations discarded from the criterion described above.

In the discrimination of longer vessels segmentations, the most selective criterion appears to be the one applied to the entire volume. Using the Matlab *regionprops3* function, the volume and the longest axis of the region under examination are obtained. The longest axis is defined for each of the three directions [x, y, z], the maximum of these three values is chosen as the diameter for a sphere that surrounds the segmented region. To discriminate the wrong segmentations, the ratio between the volume of the sphere and the volume of the segmented region is made, if this value is greater than 1, then the segmented region is discarded (Figure 36).
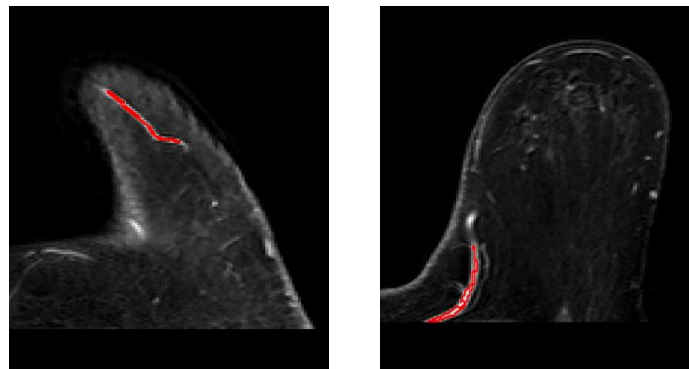
Figure 36. Examples of longer vessels segmentations discarded from the criterion described above.

3.6.2 Heuristic

As seen in the previous paragraph geometrical selection is useful for discrimination of segmentations like vessels, but this criterion is not enough for the discernment of all false positives, so a new condition has been applied.

For a further reduction of false positives, a control based on kinetic of contrast uptake in time has been implemented. In the time-signal curve are represented six points, the first point at time t = 0 corresponds to the pre-contrast scan, the following 5 points correspond to the scans after the injection of the contrast medium with a range of 90s between one

scan and the next. From this curve it is possible to obtain useful information for discriminating a lesion from a non-lesion, there are three possible cases:
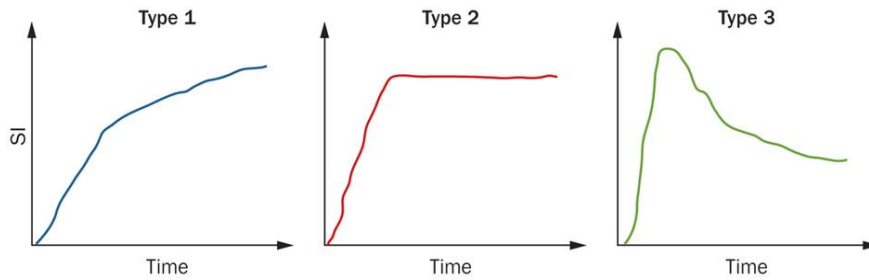
Figure 37. Contrast uptake in time possible cases.

Curve of type 1 usually belongs to benign lesions, it shows a slow uptake without washout; curve of type 3 is typical of malignant lesions, it has a fast uptake and washout. Curve of type 2 is instead a combination of the two cases mentioned and generally defines the uncertain lesion type.

In the images used in this algorithm, the contrast medium used spreads by diffusion, for this reason in the six temporal scans we cannot distinguish the wash out phase of the tissues. So, to discriminate lesions from non-lesions a control on the uptake of the curve was applied; for a greater slope of the curve, the probability that it is a tumor tissue is greater. The kinetic of contrast uptake in time was calculated for each volume, once the volume in question was selected, the average intensity value of the pixels belonging to the volume in each of the 6 corresponding time scans was calculated.
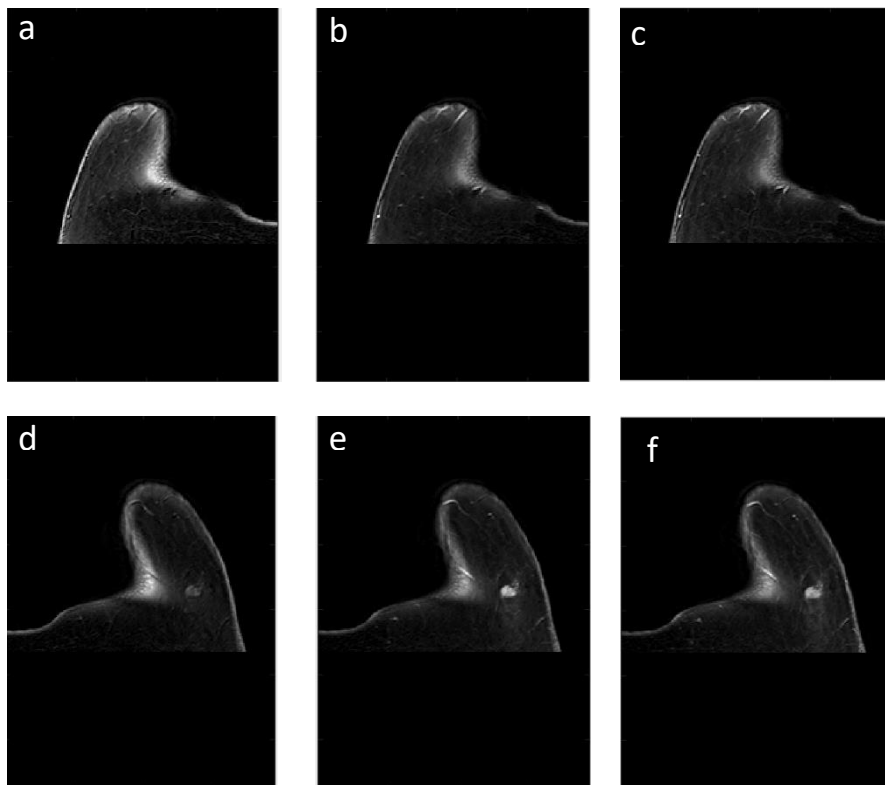
Figure 38. In the first row the images are relative to the left breast, in the second row to the right breast. (a, d) Pre-contrast injection scan. (b, e) First scan post contrast injection. (c, f) Second scan post contrast injection.

34

To evaluate the contrast absorption by the tissues under examination, the value of the first derivative was calculated between the point at t=0 and t=1 because the greater variation of tissues luminosity occurs at the first scan post injection of the gadolinium.

Figure 38 shown one example of the kinetic of contrast uptake in time, it is possible to observe how from the pre-contrast scan (d) to the first post-contrast scan (e) the tumor tissues show a noticeable change in brightness, whereas in the other tissues the brightness varies slightly. From the first post-contrast scan (e) to the second one (f) the difference in variation between tumor tissues and healthy tissues is not obvious. This confirms the validity of the choice to evaluate the difference between the pre-contrast scan and the first post contrast injection.

To select the correct threshold to discriminate tumoral tissues from healthy tissues several tests has been performed. In Figure 38, for example, Volume 1 is the healthy tissue and Volume 2 is the tumoral tissue, observing several graphs like this the value chosen for lesion discrimination is a value of first derivative equal to 22.
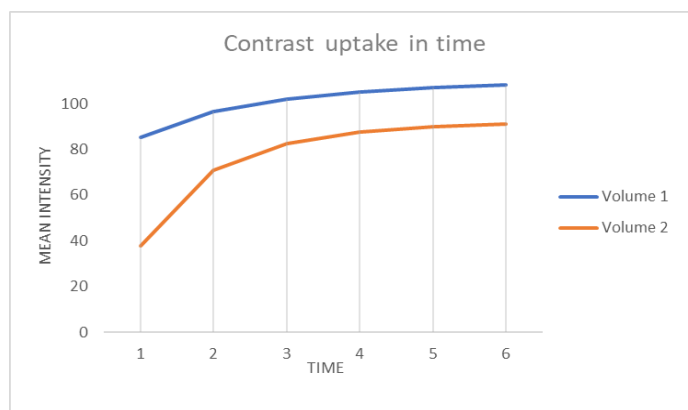

Figure 39. Contras uptake in time curve.

For values below 22 the volume under examination is discarded, otherwise the segmentation is maintained and subjected to the examination of a clinician for a more appropriate evaluation. Some examples of false positives removed by heuristic are shown in Figure 40.
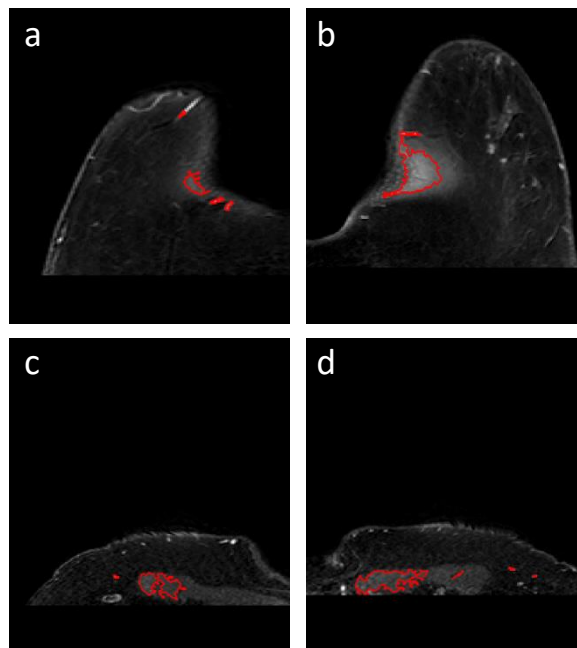

Figure 40. Wrong Seeded Region Growing.

35

Sometimes, the segmentation algorithm erroneously contours regions near the ribs (Figure 40 (c, d)), this error occurs mainly when, in the absence of the breasts, the initialized region is very close to the body.

Some of the scans provided for the construction and validation of the algorithm are post-treatment scans, applying the algorithm on these images has been observed as the thresholds set for discarding the false positives in the pre-treatment scans are too restrictive in these cases. Therefore, in post-treatment scans, a new threshold for false positives reduction has been implemented, this distinction requires an interaction with the user. Various methods have been evaluated to automatically discriminate between the two cases, but none of the variants tested has provided consistent results, so it was considered appropriate to keep the user's selection of the scan type to guarantee a lower probability of error. Unlike the condition applied in pre-treatment scans, the evaluation performed on the post-treatment images is more diversified as summarized in Table 3.

PRE-TREATMENT SCAN	POST-TREATMENT SCAN
$$\frac{d\bar{I}}{dt} < 22$$	If slice_number > 11 $$\frac{d\bar{I}}{dt} < 49$$ If slice_number <= 11 $$\frac{d\bar{I}}{dt} < 40$$

Table 3. Summary table of the conditions of discrimination of false positives

In the first column of Table 3 there is the condition for the pre-treatment scans, the first derivative between the pre-contrast injection (time 0) and the first post-contrast injection (time 1) must be higher than 22, otherwise the segmentation is deleted. For the post-treatment scan there are two conditions for two different cases, the condition applied is always relative to the first derivative, the only difference is the set thresholds. The requirement on the number of slices is an important aspect because by evaluating the average intensity on a larger number of slices the resulting value is lower than the value assumed in the case of a smaller volume. Applying only the higher threshold value set to 49 it was observed that the final result had a greater number of false positives, to reduce them without affecting the ability of the algorithm to identify the tumor tissues, it was decided to apply a double variable threshold according to the number of slices of the volume. This guarantees a better discrimination between a correct and a wrong segmentation.

Chapter 4

Image features

To aid radiologist in the analysis of the segmented region a parametrical analysis was built for each slice and for the global volume. This characterization is very useful for diagnostic purposes, the obtained parameters can provide information otherwise not obtainable from the region of interest only by observing it. Therefore, geometric variables and texture analysis were calculated to provide a set of global information about the region.

4.1 Geometrical features

Geometrical features are computed on the binary masks of the segmented regions; starting from the points of the contour, a binary mask is created with indices belonging to the contour white and the background black. To fill the form thus created, the Matlab *imfill* function is used, which generates the binary mask with the filled white object and the whole black background. In this phase the information regarding the intensity of the pixels are not necessary because the evaluation is only geometric.

Based on Huang et al. [32] we calculated the 2D and 3D parameters, values calculated are:

- Radius (R)
- Area (A)
- Spiculation (R$_s$)
- Compactness (C)
- Compactness new (C$_n$)

The 3D formulation is the following. The Radius R is

$$R = \frac{1}{n_b} \sum_{x=(i,j,k)\in boundary} \sqrt{(i-x_c)^2 + (j-y_c)^2 + (k-z_c)^2}$$

Where n_b is the number of boundary voxels and x_c, y_c and z_c are ROI center defined as

$$x_c = \frac{1}{N}\sum_{i=1}^{N} x_i \qquad\qquad y_c = \frac{1}{N}\sum_{i=1}^{N} y_i \qquad\qquad z_c = \frac{1}{N}\sum_{i=1}^{N} z_i$$

Where N is the number of pixel in the tumor (ROI). Spiculation R_s is calculated as

$$R_s = \sqrt{\frac{\sum_{x=(i,j)\in boundary}(R_x - R)^2}{n_b - 1}}$$

Where R_x is the radius for each boundary pixel. Compactness and compactness new are:

$$C = \frac{36\pi * V^2}{A^3}$$

$$C_n = \frac{n - \left(\frac{A}{6a}\right)}{n - \sqrt[3]{n^2}}$$

Where A and V denote the area, and the volume of the tumor; a is the area of one surface of a voxel, n is the number of voxels in the tumor.

For the 2D formulation Radius and Spiculation are almost similar, they lose only the z component. Compactness and Compactness new are instead remodeled as follows:

$$C = \frac{4\pi * A}{p^2}$$

$$C_n = \frac{n - \left(\frac{p}{4a}\right)}{n - \sqrt{n}}$$

Where p is the perimeter of the tumor.

4.2 Texture Analysis

MR images cannot obtain microscopic information from pixels, to increase the information obtainable from medical images the computation of a Texture Analysis (TA) is a useful method. Texture features are parameters derived from the grey-level intensity distribution, to evaluate the inter-relationship of the pixels there are several methods:

1. *Structural method* represents the geometric shape of the object using primitive geometric shapes, such as straight lines. This representation is useful for defining a synthesis of the object or to make a structural analysis.
2. *Model-based method* use mathematical models for the image analysis like fractal or stochastic, but in the parameters estimation there is a computational complexity.
3. *Statistical method* is based on the grey-level values in the medical image, this approach provides a higher indexes discrimination.
4. *Transform method* analyze the texture in different spaces, this method is base on Fourier, Gabor or Wavelet transform.

The parameters used in this work for texture analysis are:

- Histogram
- Run-length matrix (RLM)
- Co-occurrence matrix (CM)

These categories all belong to statistical class [33]. A total of 24 features are computed: *3 Global* features are computed for grey-level frequency, 8 for Grey-level Co-occurrence matrix (GLCM) and 13 for Grey-level Run-length matrix (GLRLM). To extrapolate these parameters, the ROIs are quantized on 32 grey-levels (N_g) and pixels outside the ROI are set to NaN. All the voxels inside the ROI with a value outside the range $\mu \pm 3\sigma$ are rejected to make texture measurements more consistent [34].

Histogram is the count of how many pixels have the same grey-level value in an image. To obtain ROI histogram the Matlab function *hist* is implemented, the convention is to set the lower values to darker gray-level, and the higher value to lighter gray-level. In this case the 0 value denotes the black, the number of gray levels normalization N_g denotes the white. X coordinate represents the intensity values of the pixels, y coordinate represents the corresponding number of pixels. From histogram many parameters can be obtained, we calculated *Variance*, *Skewness* and *Kurtosis*.

Co-occurrence matrix is a technique for the extraction of statistical information from the image. It is based on the observation of intensity pixels value distribution, the matrix count pairs of pixel having the same grey-level distribution. There may be different co-occurrence matrix, one for each direction: horizontal, vertical and two main diagonals directions.
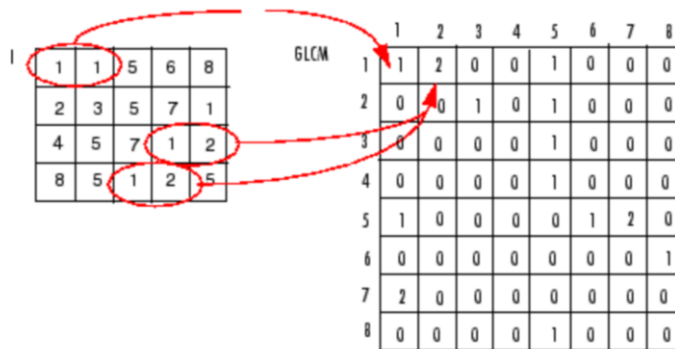
Figure 41. Grey-level co-occurrence matrix computation. On the left there is the original grey level distribution, on the right is represented the GLCM matrix.

Figure 41 shown one example of the GLCM matrix calculation, starting from the 4x5 image I on the left the GLCM values are obtained. The element (1,1) in the GLCM has the value 1 because there is only one pair in the image where two horizontal adjacent pixels have both value 1. Element (1,2) has value 2 because two pair in the image have the adjacent value 1 and 2. In summary, matrix value $P_{i,j}$ is the number of times pixel with grey level *i* has a neighbor with grey level *j*.

In this study, GLCM is a 32x32 matrix, based on 32 grey levels, computed adding up the frequency of co-occurrence of all pixels with distance d=1 in the horizontal (0°), vertical (90°) and two main diagonals (45° - 135°) directions. All GLCM parameters are reported in Table 2 and explained in Appendix A.

Run-length matrix measures for each gray level value the number of times it occurs that two or more pixels of the same value are adjacent. There may be different run-length

matrix, one of each pair of distances and directions. The range of distances usually varies from 1 to 5 pixels in the horizontal, vertical and two main diagonals directions.
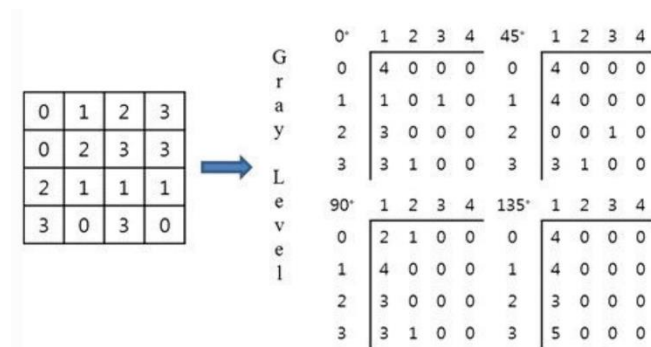

Figure 42. Grey-level run length matrix computation. On the left there is the original grey level distribution, on the right is represented the GRLM matrix in the four main directions.

Figure 42 shown one example of GRLM computation in the four main directions for distances equal to 1, 2, 3 and 4. Matrix element $P_{i,j}$ represents the number of time a segment with intensity i is as longest j pixels.

GLRLM is a 32xj matrix, where j is the longest available run. Segment frequencies are summed up in all directions. All GLRM parameters are reported in Table 4 and explained in Appendix A [33].
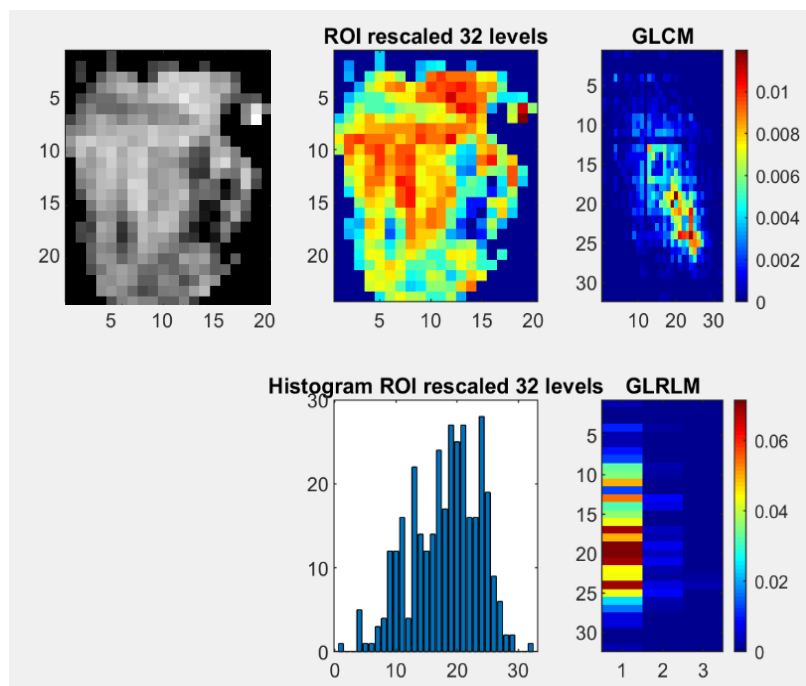
Figure 43. Imaging features extrapolations: the defined ROI (first column) is discretized to 32 grey level (second column up). Global features are derived from frequency grey-level histogram (second column down). Grey-Level Co-Occurence Matrix (GLCM, third column up) and Grey-Level Run-Length Matrix (GLRLM third column down) are used for second order TA feature calculation.

Imaging features

Geometrical

1	Compactness new	*Measure of deviation from regular square shape*
2	Compactness	*Measure of deviation from regular circle shape*
3	Radius	
4	Spiculation	*Measure of margin irregularity*
5	Area	

TA Global

|		
6	Variance	*Measure of grey level frequency homogeneity*
7	Skewness	*Measure of histogram asymmetry*
8	Kurtosis	*Measure of histogram "peakedness"*

TA GLCM

9	Energy	*Measure of local uniformity of grey levels*
10	Contrast	*Measure of the amount of grey levels*
11	Entropy	*Measure of randomness of grey levels*
12	Homogeneity	*Measure of local homogeneity, higher with less contrast*
13	Correlation	*Measure of neighboring pixel grey level linear dependency*
14	Sum Average	*Measure of overall image brightness*
15	Dissimilarity	*Measure of spread out of grey levels sum of pixel pair*
16	Variance GLCM	*Measure of deviation from average values*

TA GLRLM

17	SRE	*Short Run Emphasis*
18	LRE	*Long Run Emphasis*
19	GLN	*Grey-Level Nonuniformity*
20	RLN	*Run-Length Nonuniformity*
21	RP	*Run Percentage*
22	LGRE	*Low Grey-Level Run Emphasis*
23	HGRE	*High Grey-Level Run Emphasis*
24	SRLGE	*Short Run Low Grey-Level Emphasis*
25	SRHGE	*Short Run High Grey-Level Emphasis*
26	LRLGE	*Long Run Low Grey-Level Emphasis*
27	LRHGE	*Long Run High Grey-Level Emphasis*
28	GLV	*Grey-Level Variance*
29	RLV	*Run-Length Variance*

Table 4. All collected features. TA = Texture Analysis. GLCM = Grey-Level Co-Occurence Matrix. GLRLM = Grey-Level Run Length Matrix

Chapter 5

Validations

For the algorithm validation, 5 patients are provided by Borgo Trento Hospital in Verona, of these 5 patients we have several post-treatment examinations, 10 in total. The purpose of this phase is to evaluate the algorithm performances both on pre-treatment images and post-treatment images. The last ones are acquired exactly like the first type, the only differences between the two is that in a post-treatment patient the luminance of the tumoral tissue is lower, so the values of the threshold in the algorithm must be readjusted to ensure coherence with the new images. For this reason, a new correction for false positives reduction has been implemented; the operations of the two methods are the same, the only variable are the thresholds (see Paragraph 3.6.2).

For the algorithm validation two main approaches were adopted: a first analysis was carried out to evaluate the ability of the algorithm to recognize the lesions, afterwards we focused on the evaluation of segmentation quality, it means how accurate was the region contouring compared to that of two operators supervised by an expert.

The main objective adopted in the realization of the algorithm is to guarantee the greatest possible coverage in terms of lesions recognition, also to the detriment of a greater number of false positives. To evaluate the algorithm's effectiveness in terms of recognizing suspect regions we classify all region segmented in three main categories:

- *True Positive* (TP) corresponds to the correct identification and segmentation of the tumor region;
- *False Positive* (FP) is the wrong segmentation of a healthy tissue that can be a vessel, an internal organ or areas affected by noise;
- *False Negative* (FN) is recognized as the failure to segment a tissue that is identified as suspected by an expert.

Given this classification, two main parameters were used defined in [35]:

- *Precision* is the number of correct segmentation divided by the number of all segmented regions:

$$Precision = \frac{TP}{TP + FP}$$

- *Recall*, also called sensitivity, is the number of correct segmentation divided by the number of the segmentations that should be returned:

$$Recall = \frac{TP}{TP + FN}$$

These two values are useful to obtain a curve, called PR curve, which is an alternative approach to ROC curve for evaluating the segmentation performances. The PR curve focuses on the algorithm's ability to detect lesions in mammary MRI, but it ignores the accuracy of the region contouring. So, to give a more complete evaluation of the algorithm performances, further parameters are computed.

To provide a statistical validation of image segmentation we referred to Snekha Thakran et al [36], they propose the Dice Similarity Coefficient (DSC) and Jaccard coefficient; to compute these parameters a manual segmentation is needed. DSC is used as spatial overlap index, to compare the automated and the manual segmentation:

$$DSC(A, B) = \frac{2 * (A \cap B)}{A + B}$$

Where A is the manual segmentation and B the automated segmentation, $\cap$ is the intersection between the two segmented areas. This index ranges from 0 to 1, 0 indicates no overlap between the two segmentations, and 1 indicates the complete overlap.

The other parameter calculated for the evaluation of the segmentation accuracy is the Jaccard coefficient, the formulation is the following:

$$Jaccard\ Coefficient = \frac{|A \cap B|}{|A| + |B| - |A \cap B|}$$

Like in the Dice Coefficient, A is the manual segmentation and B the automated segmentation. This value also provides an evaluation of the similarity between the two segmentations, given the manual segmentation A and the automated segmentation B several parameters are computed to give a more complete evaluation of the segmentation accuracy, like reported in [16]:

- Sensitivity

$$Sensitivity = \frac{|A \cap B|}{|B|}$$

- Specificity

$$Specificity = \frac{|A - B|}{|A|}$$

5.1 Results

The algorithm was applied to the 15 exams provided for validation. For each of these exams the volume consisted of 195 slices, so the algorithm was tested overall on 2925 images. The performances of the algorithm were evaluated in terms of true positives, false positives and false negatives. The results obtained are shown in Table 5:

	Values
True positives	456
False positives	10
False negatives	75

Table 5. Results of algorithm segmentation.

The priority of the algorithm was to outline all the suspicious regions present even at the expense of a greater number of false positives. As can be seen from the results obtained, the false positives are far below the true positives, evaluating the implications of the false negatives, it has been observed that most of them belong to the outermost slices of the segmented volumes, which does not imply a lack of recognition of the suspect region. To evaluate the algorithm's effectiveness in terms of recognizing suspect regions we calculated precision and recall values:

Precision	0,978540773
Recall	0,858757062

*Table 6.* Precision and Recall results.

From the value resulting it is possible to observe a good ability to recognize suspicious tissues (about 98%), which was the main purpose in this phase of analysis; the algorithm also guarantees a higher probability of recognizing true positives despite other segmentation errors.

These values, however, do not give any information on the accuracy of the segmentation, in order to have an overall evaluation of the algorithm's performance a subsequent evaluation to the segmentation has been added. To do this, it was necessary to manually segment the images, the software used for the manual segmentation was 3D Slicer. A sample of 31 images were randomly selected from the 15 available exams to ensure the greatest variability. To evaluate the intra- and inter-operator variability two operator have been selected, the manual segmentations were subsequently evaluated by an expert to ensure greater validity of the results obtained.

The computed parameters are the Dice and Jaccard coefficients. Observing the results coefficient of all single manual segmentations greater performances was detected in pre-treatment scans compared to post-treatment, the most evident variation has been seen in the Dice and Jaccard coefficients. Figure 44 shown the boxplot of the two operator's segmentations, the boxplot shown the variability of the obtained values in the different slices segmentation.
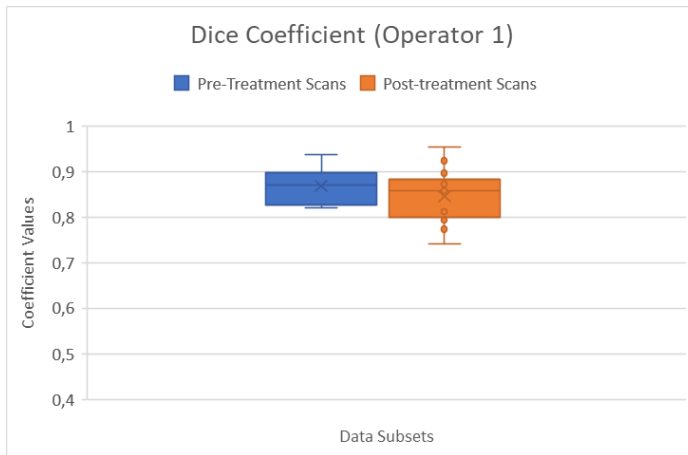
(a) Boxplot of the Dice Coefficient of Operator 1 segmentations.
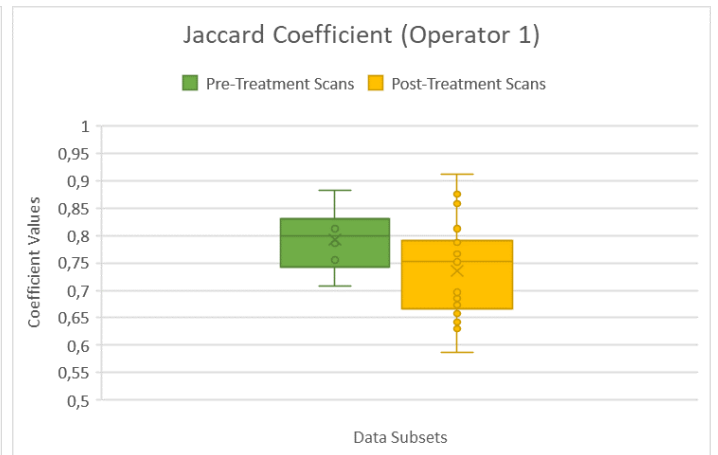
(b) Boxplot of the Jaccard Coefficient of Operator 1 segmentations.
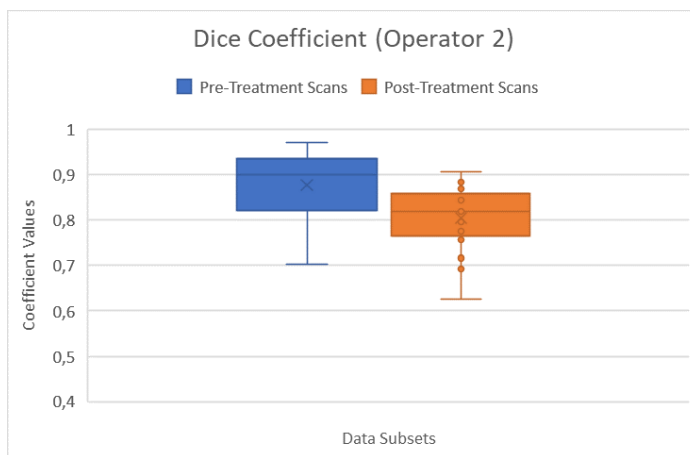
(c) Boxplot of the Dice Coefficient of Operator 2 segmentations.
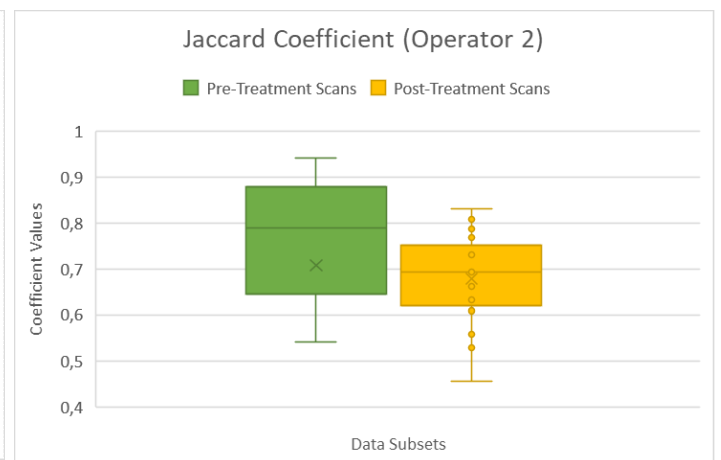
(d) Boxplot of the Jaccard Coefficient of Operator 2 segmentations.

Figure 44. Boxplot of the Dice and Jaccard coefficients of the two operator's segmentations.

For both operators the maximum and median value of the parameters obtained in the pre-treatment segmentation are greater than the post-treatment segmentation, this means that in the scans before the application of neoadjuvant therapy, the algorithm presents a greater precision in the recognition of the suspect regions contours.

The greatest differences can be seen for Operator 2, the values obtained for the pre-treatment scans are so much greater than the values obtained in the post-treatment segmentations, the variation is about the 7.2% for the mean Dice coefficient and 10.7% for the mean Jaccard coefficient. For Operator 1 the variability between pre and post treatment seems minimal, the most evident is the Jaccard coefficient, it has a median value greater for the pre-treatment scans of about 5.7%.

For both operator we can observe as the post-treatment segmentation values have a lot of outliers compared to the pre-therapy values, this means that the segmentation algorithm in post-treatment cases is not as solid as in the pre-treatment cases. This variability, as already mentioned above, is mainly linked to the effects of therapy. After a chemotherapeutic treatment the contours of the tumor tissues no longer have a clearly defined shape, for this reason the operator segmentation variability is greater because some operators (Operator 1) segment only the brightest region, others (Operator 2) on the

other hand tend to overestimate the region of interest also surrounding bordering regions with little perfusion.

To give an overall evaluation of the segmentation algorithm performances, in addition to the Dice and Jaccard coefficients also sensitivity and specificity are computed. Of all these values the mean and standard deviation values have been calculated and the maximum and minimum values have been reported to guarantee a complete evaluation:

OPERATOR 1	DSC	Jaccard Coefficient	Sensitivity	Specificity
Mean	0,870213661	0,772714098	0,83138663	0,185589754
Standard Deviation	0,042905925	0,067989656	0,08712151	0,096362259
Max	0,954180444	0,91237579	0,97709924	0,379746835
Min	0,808510638	0,678571429	0,69556025	0,021967526

Table 7. Manual segmentation results for Operator 1.

OPERATOR 2	DSC	Jaccard Coefficient	Sensitivity	Specificity
Mean	0,854519	0,748585	0,818854	0,18365
Standard Deviation	0,063806	0,183179	0,124711	0,132838
Max	0,969644	0,941077	1	0,448819
Min	0,691806	0	0,536558	0,00117

Table 8. Manual segmentation results for Operator 2.

In Table 7 and Table 8 we can see the result value of all image segmented, both pre- and post- treatment scans; the overall results obtained for both operators show how the algorithm is consistent with the evaluations carried out by the operators. Values of Dice coefficient greater then 0.7 are considered a good overlap for image segmentation, Jaccard coefficient has lower value than DSC but it is still a good result. In the tables are also shown the value of Sensitivity and Specificity of the automatic segmentation, these ranges from 0.53 to 1 for the sensitivity and 0.001 to 0.44 for the specificity. The values between the two operators are overall comparable, but we can observe the variability of the standard deviation, operator 1 has a lower value than the operator 2, this is probably related to the post-treatment scans variability.

Chapter 6

Conclusions

In this study it was proposed a fully automated system for lesion identification and segmentation on Mammary Magnetic Resonance Images. The algorithm works individually on each slice and then considerations are made on the reconstructed volumes. Starting from the proposed algorithm [16], a series of changes have been made to compensate the recognition and segmentation errors found.

The user must select the folder containing the DCE images and then the algorithm performs the operations explained previously, at the end of the computation, on the recognized volumes a parametric characterization, useful for diagnostic purposes, is provided both on 2D and 3D setup.

Algorithm run about 5-8 minutes for the complete volume scanning, at the end of the computation all images segmented are saved in a folder called '*Img_segmented*' and all parameters useful for the tissue characterization are saved in a '*Data.xlsx*' file.

The advantages of the algorithm are the following:

1. Fully automated identification and segmentation algorithm
2. Low number of false positives
3. Low computational times
4. Results not dependent from the operator
5. Automatic computation of geometrical features and Texture Analysis

The lesion detection system created has a precision value of 98% with a low number of false positives. The segmentation algorithm shows a great compatibility in the pre-treatment images with a Dice coefficient equal to 87%, in the post-neoadjuvant therapy results seems less performing because the region of interest contour is not well defined. This limitation isn't a clinical problem, the main purpose of the project was to identify the suspect tissues and deliver an overall assessment of the extension of the tumor region, also providing additional clinical parameters for the valuation of tissue malignancy. Since several tests of the same patient were provided, even after some sessions of neoadjuvant therapy, it was possible to observe how the algorithm was able to monitor the effectiveness of the therapy over time, providing not only a geometric evaluation of the

residual but also a parametric region evaluation, with a series of texture analysis features useful for providing a more complete evaluation.

The results obtained therefore respect the required expectations, of course the performances of the system can be improved: the segmentations of the post-therapy tissue can be enhanced reshaping the selection of thresholds and adjusting post-treatment images pre-processing, the number of false positives can be further reduced with a more accurate discrimination criterion and also the computational time can be improved optimizing the Matlab script or transferring the codes to a more optimized platform.

Appendix A

Texture Analysis Features

A.1 Global texture features

For the *Global* features computation, a frequency histogram is defined. *P(i)* is the number of pixels with grey-level *I*; *i* ranges from 1 to N_g where N_g is the number of grey-level normalization:

$$p(i) = \frac{P(i)}{\sum_{i=1}^{N_g} P(i)}$$

The *Global* texture features are:

- Variance:

$$\sigma^2 = \sum_{i=1}^{N_g} (i - \mu)^2 \, p(i)$$

- Skewness:

$$s = \sigma^{-3} \sum_{i=1}^{N_g} (i - \mu)^3 \, p(i)$$

- Kurtosis:

$$k = \sigma^{-4} \sum_{i=1}^{N_g} [(i - \mu)^4 \, p(i)] - 3$$

A.2 Grey-level Co-occurrence Matrix (GLCM) texture features

The GLCM texture features need the GLCM computation of the quantized region of interest (ROI). N_g is the number of quantized grey-level, GLCM has size N_g x N_g where $P(i, j)$ represents the number of times a pixel of intensity i is near a pixel with intensity j in the ROI. Only one GLCM is computed per ROI by adding up the co-occurrence matrix of all main directions. Pixel outside ROI were defined as NaN to not influence the features computation. $p(i, j)$ pixel of normalized GLCM is defined as:

$$p(i,j) = \frac{P(i,j)}{\sum_{i=1}^{N_g} \sum_{i=1}^{N_g} P(i,j)}$$

The quantities needed for GLCM features computation are the following:

$$\mu_i = \sum_{i=1}^{N_g} i \sum_{j=1}^{N_g} p(i,j), \qquad \mu_j = \sum_{j=1}^{N_g} j \sum_{i=1}^{N_g} p(i,j)$$

$$\sigma_i = \sum_{i=1}^{N_g} (i - \mu_i)^2 \sum_{j=1}^{N_g} p(i,j), \qquad \sigma_i = \sum_{j=1}^{N_g} (j - \mu_j)^2 \sum_{i=1}^{N_g} p(i,j)$$

The GLCM texture features are then defined as:

- Energy:

$$Energy = \sum_{i=1}^{N_g} \sum_{j=1}^{N_g} [p(i,j)]^2$$

- Contrast:

$$Contrast = \sum_{i=1}^{N_g} \sum_{j=1}^{N_g} (i-j)^2 p(i,j)$$

- Correlation:

$$Correlation = \sum_{i=1}^{N_g} \sum_{j=1}^{N_g} \frac{(i - \mu_i)(j - \mu_j) p(i,j)}{\sigma_i \sigma_j}$$

- Homogeneity:

$$Homogeneity = \sum_{i=1}^{N_g} \sum_{j=1}^{N_g} \frac{p(i,j)}{1 + |i - j|}$$

- Variance:

$$VarianceGLCM = \frac{1}{N_g \text{ x } N_g} \sum_{i=1}^{N_g} \sum_{j=1}^{N_g} [(i - \mu_i)^2 p(i,j) + (j - \mu_j)^2 p(i,j)]$$

- Sum Average:

$$Sum\ Average = \frac{1}{N_g \text{ x } N_g} \sum_{i=1}^{N_g} \sum_{j=1}^{N_g} [ip(i,j) + jp(i,j)]$$

- Entropy:

$$Entropy = -\sum_{i=1}^{N_g} \sum_{j=1}^{N_g} p(i,j) log_2(p(i,j))$$

- Dissimilarity:

$$Dissimilarity = \sum_{i=1}^{N_g} \sum_{j=1}^{N_g} |i - j| p(i,j)$$

A.3 Grey-level Run-Length Matrix (GLRLM) texture features

The GLRLM texture features need the GLRLM computation of the quantized region of interest (ROI). *P(i, j)* represents the number of pixel of grey-level *i* and of length *j* in the ROI. Matrix size is N_g x L_r where N_g is the number of grey-level quantization, L_r is the longest run of any grey-level in the ROI. The GLRLM is obtained adding up all possible longest run-length in all the directions. *p(i, j)* of the normalized GLRLM is defined as:

$$p(i,j) = \frac{P(i,j)}{\sum_{i=1}^{N_g} \sum_{j=1}^{L_r} P(i,j)}$$

For the GLRLM texture features the following quantities are required:

$$\mu_i = \sum_{i=1}^{N_g} i \sum_{j=1}^{L_r} p(i,j), \qquad \mu_j = \sum_{j=1}^{L_r} j \sum_{i=1}^{N_g} p(i,j)$$

The GLRLM texture features are defined as:

- Short Run Emphasis (SRE):

$$SRE = \sum_{i=1}^{N_g} \sum_{j=1}^{L_r} \frac{p(i,j)}{j^2}$$

- Long Run Emphasis (LRE):

$$LRE = \sum_{i=1}^{N_g} \sum_{j=1}^{L_r} j^2 p(i,j)$$

- Grey-Level Nonuniformity (GLN):

$$GLN = \sum_{i=1}^{N_g} \left(\sum_{j=1}^{L_r} p(i,j) \right)^2$$

- Run-Length Nonuniformity (RLN):

$$RLN = \sum_{j=1}^{L_r} \left(\sum_{i=1}^{N_g} p(i,j) \right)^2$$

- Run Percentage (RP):

$$RP = \frac{\sum_{i=1}^{N_g} i \sum_{j=1}^{L_r} p(i,j)}{\sum_{j=1}^{L_r} j \sum_{i=1}^{N_g} p(i,j)}$$

- Low Grey-Level Run Emphasis (LGRE):

$$LGRE = \sum_{i=1}^{N_g} \sum_{j=1}^{L_r} \frac{p(i,j)}{i^2}$$

- High Grey-Level Run Emphasis (HGRE):

$$HGRE = \sum_{i=1}^{N_g} \sum_{j=1}^{L_r} i^2 p(i,j)$$

- Short Run Low Grey-Level Emphasis (SRLGE):

$$SRLGE = \sum_{i=1}^{N_g} \sum_{j=1}^{L_r} \frac{p(i,j)}{i^2 j^2}$$

- Short Run High Grey-Level Emphasis (SRHGE):

$$SRHGE = \sum_{i=1}^{N_g} \sum_{j=1}^{L_r} \frac{i^2 p(i,j)}{j^2}$$

- Long Run Low Grey-Level Emphasis (LRLGE):

$$LRLGE = \sum_{i=1}^{N_g} \sum_{j=1}^{L_r} \frac{j^2 p(i,j)}{i^2}$$

- Long Run High Grey-Level Emphasis (LRHGE):

$$LRHGE = \sum_{i=1}^{N_g} \sum_{j=1}^{L_r} i^2 j^2 p(i,j)$$

- Grey-Level Variance (GLV):

$$GLV = \frac{1}{N_g \times L_r} \sum_{i=1}^{N_g} \sum_{j=1}^{L_r} (i\, p(i,j) - \mu_i)^2$$

- Run-Length Variance (RLV):

$$RLV = \frac{1}{N_g \times L_r} \sum_{i=1}^{N_g} \sum_{j=1}^{L_r} (j\, p(i,j) - \mu_j)^2$$

REFERENCES

[1]   C. P. Stewart, Bernard W, Wild, "International Agency for Research on cancer. World Health Organizarion. World cancer report 2014. World cancer Report 2014.," *2014*, no. 1, p. 630, 2014.

[2]   A. Lundqvist, E. Andersson, I. Ahlberg, M. Nilbert, and U. Gerdtham, "Socioeconomic inequalities in breast cancer incidence and mortality in Europe—a systematic review and meta-analysis," *Eur. J. Public Health*, vol. 26, no. 5, pp. 804–813, 2016.

[3]   C. E. Desantis, S. A. Fedewa, A. G. Sauer, J. L. Kramer, R. A. Smith, and A. Jemal, "Breast Cancer Statistics , 2015 : Convergence of Incidence Rates Between Black and White Women," *A cancer J. Clin.*, vol. 66, no. 1, pp. 31–42, 2016.

[4]   S. Harms, "Breast Magnetic Resonance Imaging," *Semin Ultrasound CT MR*, vol. 19, no. 1, pp. 104–120, 1998.

[5]   O. Faust, U. R. Acharya, and T. Tamura, "Formal design methods for reliable computer-aided diagnosis: A review," *IEEE Rev. Biomed. Eng.*, vol. 5, pp. 15–28, 2012.

[6]   G. Ertaş, H. Ö. Gülçür, O. Osman, O. N. Uçan, M. Tunaci, and M. Dursun, "Breast MR segmentation and lesion detection with cellular neural networks and 3D template matching," *Comput. Biol. Med.*, vol. 38, no. 1, pp. 116–126, 2008.

[7]   M. Tang, "Edge Detection and Image Segmentation Based on Cellular Neural Network," *2009 3rd Int. Conf. Bioinforma. Biomed. Eng.*, pp. 1–4, 2009.

[8]   J. Yao, J. Chen, and C. Chow, "Breast Tumor Analysis in Dynamic Contrast Enhanced MRI Using Texture Features and Wavelet Transform," *IEEE J. Sel. Top. Signal Process.*, vol. 3, no. 1, pp. 94–100, 2009.

[9]   Q. Wu, M. Salganicoff, A. Krishnan, D. S. Fussell, and M. K. Markey, "Interactive lesion segmentation on dynamic contrast enhanced breast MRI using a Markov model," 2006, vol. 6144, p. 61444M.

[10]   G. Ertas, S. J. Doran, and M. O. Leach, "A computerized volumetric segmentation method applicable to multi-centre MRI data to support computer-aided breast tissue analysis, density assessment and lesion localization," *Med. Biol. Eng. Comput.*, vol. 55, no. 1, pp. 57–68, 2017.

[11]   S. Vesal, N. Ravikumar, S. Ellman, and A. Maier, "Comparative analysis of unsupervised algorithms for breast MRI lesion segmentation," *Inform. aktuell*, no. 211279, pp. 257–262, 2018.

[12]   R. Azmi, N. Norozi, R. Anbiaee, L. Salehi, and A. Amirzadi, "IMPST: A New Interactive Self-Training Approach to Segmentation Suspicious Lesions in Breast MRI.," *J. Med. Signals Sens.*, vol. 1, no. 2, pp. 138–48, May 2011.

[13]   A. Vignati *et al.*, "Performance of a fully automatic lesion detection system for breast DCE-MRI," *J. Magn. Reson. Imaging*, vol. 34, no. 6, pp. 1341–1351, 2011.

[14]   D. M. Renz *et al.*, "Detection and classification of contrast-enhancing masses by a fully automatic computer-assisted diagnosis system for breast MRI," *J. Magn. Reson. Imaging*, vol. 35, no. 5, pp. 1077–1088, 2012.

[15]   A. Gubern-Mérida *et al.*, "Automated localization of breast cancer in DCE-MRI," *Med. Image Anal.*, vol. 20, no. 1, pp. 265–274, 2015.

[16]   A. Q. Al-Faris, U. K. Ngah, N. A. M. Isa, and I. L. Shuaib, "Computer-aided segmentation system for breast MRI tumour using modified automatic seeded region growing (BMRI-MASRG)," *J. Digit. Imaging*, vol. 27, no. 1, pp. 133–144, 2014.

[17]   S. T. Ligthart *et al.*, "Circulating Tumor Cells Count and Morphological Features in Breast, Colorectal and Prostate Cancer," *PLoS One*, vol. 8, no. 6, p. e67148, 2013.

[18]   N. A. de Glas *et al.*, "Contralateral breast cancer risk in relation to tumor morphology and age—in which patients is preoperative MRI justified?," *Breast Cancer Res. Treat.*, vol. 150, no. 1, pp. 191–198, 2015.

[19]   M. Fan, H. Li, S. Wang, B. Zheng, J. Zhang, and L. Li, "Radiomic analysis reveals DCE-MRI features for prediction of molecular subtypes of breast cancer," *PLoS One*, vol. 12, no. 2, pp. 1–15, 2017.

[20]   T. Kagawa *et al.*, "Basic principles of magnetic resonance imaging for beginner oral and maxillofacial radiologists," *Oral Radiol.*, vol. 33, no. 2, pp. 92–100, 2017.

[21]   G. Petralia, L. Bonello, F. Priolo, P. Summers, and M. Bellomi, "Breast MR with special focus on DW-MRI and DCE-MRI," *Cancer Imaging*, vol. 11, no. 1, pp. 76–90, 2011.

[22]   C.-H. Wang, "Review of treatment assessment using DCE-MRI in breast cancer radiation therapy," *World J. Methodol.*, vol. 4, no. 2, p. 46, 2014.

[23]   D. Mariotti, "Risonanza magnetica della mammella TSRM e QUALITÀ nel percorso senologico: QUALI REALTÀ POSSIBILI IN ITALIA?," 2014.

[24]   I. Thomassin-Naggara, I. Trop, L. Lalonde, J. David, L. Péloquin, and J. Chopier, "Tips and techniques in breast MRI," *Diagn. Interv. Imaging*, vol. 93, no. 11, pp. 828–839, 2012.

[25]   L. A. Tudorica *et al.*, "A feasible high spatiotemporal resolution breast DCE-MRI protocol for clinical settings," *Magn. Reson. Imaging*, vol. 30, no. 9, pp. 1257–1267, 2012.

[26]   E. A. M. O'Flynn and N. M. DeSouza, "Functional magnetic resonance: biomarkers of response in breast cancer.," *Breast Cancer Res.*, vol. 13, no. 1, p. 204, Feb. 2011.

[27]   M.-A. Weber, *Magnetic resonance imaging of the skeletal musculature.* .

[28]   J. P. B. O. Connor, P. S. Tofts, K. A. Miles, G. Thompson, and A. Jackson, "Dynamic contrast-enhanced imaging techniques : CT and MRI," vol. 84, 2011.

[29]   A. Release, "Application Guide," vol. 1.

[30]   Chunming Li, Chenyang Xu, Changfeng Gui, and M. D. Fox, "Level Set Evolution without Re-Initialization: A New Variational Formulation," *2005 IEEE Comput. Soc. Conf. Comput. Vis. Pattern Recognit.*, vol. 1, pp. 430–436, 2005.

[31]   C. Li, C. Xu, C. Gui, and M. D. Fox, "Distance regularized level set evolution and its application to image segmentation," *IEEE Trans. Image Process.*, vol. 19, no. 12, pp. 3243–3254, 2010.

[32]   Y. H. Huang, Y. C. Chang, C. S. Huang, T. J. Wu, J. H. Chen, and R. F. Chang, "Computer-aided diagnosis of mass-like lesion in breast MRI: Differential analysis of the 3-D morphology between benign and malignant tumors," *Comput. Methods Programs Biomed.*, vol. 112, no. 3, pp. 508–517, 2013.

[33]   G. Castellano, L. Bonilha, L. M. Li, and F. Cendes, "Texture analysis of medical images," *Clin. Radiol.*, vol. 59, no. 12, pp. 1061–1069, 2004.

[34]   M. Vallières, C. R. Freeman, S. R. Skamene, and I. El Naqa, "A radiomics model from joint FDG-PET and MRI texture features for the prediction of lung metastases in soft-tissue sarcomas of the extremities," *Phys. Med. Biol.*, vol. 60, no. 14, pp. 5471–5496, 2015.

[35]   B. Ozenne, F. Subtil, and D. Maucort-Boulch, "The precision-recall curve overcame the optimism of the receiver operating characteristic curve in rare diseases," *J. Clin. Epidemiol.*, vol. 68, no. 8, pp. 855–859, 2015.

[36]   S. Thakran, S. Chatterjee, M. Singhal, R. K. Gupta, and A. Singh, "Automatic outer and inner breast tissue segmentation using multi-parametric MRI images of breast tumor patients," *PLoS One*, vol. 13, no. 1, pp. 1–21, 2018.